Experimental Eye Research

Ionizing radiation causes vision impairment in neonatal B6C3F1 mice

--Manuscript Draft--

Manuscript Number:	YEXER_2020_40R3
Article Type:	Research Paper
Keywords:	Cataracts; OCT; ionizing radiation; Scheimpflug Imaging; retina; visual acuity; eye lens
Corresponding Author:	Claudia Dalke Helmholtz Zentrum München Neuherberg, Germany
First Author:	Daniel Pawliczek
Order of Authors:	Daniel Pawliczek
	Helmut Fuchs
	Valerie Gailus-Durner
	Martin Hrabé de Angelis
	Jochen Graw
	Claudia Dalke
Abstract:	Ionizing radiation interacts with lenses and retinae differently. In human lenses, posterior subcapsular cataracts are the predominant observation, while retinae are comparably resistant even to relatively high doses. Here we demonstrate the effects of 2 Gy of low linear energy transfer ionizing radiation on eyes of neonatal B6C3F1 mice. Optical coherence tomography and Scheimpflug imaging were used the first time to monitor mouse lenses and retinae in vivo, visual acuity of mice was determined and histological analysis was conducted. Our results show that around 9 months after irradiation visual acuity was reduced by up to 50% in irradiated mice. Vision impairment was caused by retinal atrophy and inner cortical cataracts. These results help to further understanding of the ionizing radiation risks for human foeti (8 month), that match eye development stages in neonatal mice.
Response to Reviewers:	We thank the reviewer for reading and commenting our manusript. Our answers are given point by point in the review report.

Ionising Radiation Causes Vision Impairment in Neonatal B6C3F1 Mice

Daniel Pawliczek[a], Helmut Fuchs[b], Valerie Gailus-Durner[b], Martin Hrabě de Angelis[b,c,d], Jochen Graw[a], Claudia Dalke[a,e,*]

[a]*Helmholtz Zentrum München GmbH - German Research Center for Environmental Health, Institute of Developmental Genetics, Neuherberg, Germany*
[b]*Helmholtz Zentrum München GmbH - German Research Center for Environmental Health, Institute of Experimental Genetics, Neuherberg, Germany*
[c]*Chair of Experimental Genetics, School of Life Science Weihenstephan, Technische Universität München, Freising, Germany*
[d]*German Center for Diabetes Research (DZB), Neuherberg, Germany*
[e]*Present address: Helmholtz Zentrum München GmbH - German Research Center for Environmental Health, Institute of Metabolism and Cell Death, Neuherberg, Germany*

Abstract

Ionising radiation interacts with lenses and retinae differently. In human lenses, posterior subcapsular cataracts are the predominant observation, whereas retinae of adults are comparably resistant to even relatively high doses. In this study, we demonstrate the effects of 2 Gy of low linear energy transfer ionising radiation on eyes of B6C3F1 mice aged postnatal day 2. Optical coherence tomography and Scheimpflug imaging were utilised for the first time to monitor murine lenses and retinae *in vivo*. The visual acuity of the mice was determined and histological analysis was conducted. Our results demonstrated that visual acuity was reduced by as much as 50 % approximately 9 months after irradiation in irradiated mice. Vision impairment was caused by retinal atrophy and inner cortical cataracts. These results help to further our understanding of the risk of ionising radiation for human foeti (∼ 8 mo), which follow the same eye development stages as neonatal mice.

Keywords: cataracts, eye lens, ionising radiation, OCT, retina, Scheimpflug imaging, visual acuity

1. Introduction

Low linear energy transfer (LET) ionising radiation (IR) is hypothesised to induce lens alterations (cataracts) arising from genetic damage caused in the epithelial cells, implying the causality of genetic misrepair and subsequently failing differentiation of epithelial cells to organelle-free fibre cells [Ainsbury et al., 2016]. At the same time, IR induces oxidation processes detrimental to the lens [Uwineza et al., 2019].

Gajewski et al. [1977] meticulously analysed the correlation between different mouse ages (inbred A strain) at irradiation with 300 R (∼ 2.88 Gy) of x-rays and the occurrence of 2 cataract types that distinguish themselves by the onset changes in the posterior lens cortex. They revealed that punctual opacities in the 'lower region of the posterior cortex' appeared mainly mice irradiated after P3 (type II), while 'opaque strands running from the periphery of a lens' (type I) appeared as typical phenotype in mice irradiated at ages younger than P3. In 96.7 % of the mice irradiated at postnatal day 2 (P2) a stage 1 cataract or worse was observed. The median time for stage 1-3 type I cataracts in P2 mice was between 100 and 180 days. Older animals developed far later type II cataracts of those stages, with differences being more drastic the higher the respective cataract stages.

In a later study by De Stefano et al. [2015], a similar effect of radiation sensitivity was observed in P2-irradiated mice of the CD1 strain exposed to a dose of 3 Gy. Of the mice examined macroscopically, 10.18 % formed either uni- or bilateral cataracts with a median latency of 9.5

*Corresponding author
Email address: claudia.dalke@helmholtz-muenchen.de (Claudia Dalke)

weeks, whereas controls or irradiated mice at P56 displayed a cataract incidence of 0 %. This corroborated the results of the former study perfectly.

Both studies presented data suggesting that the earlier mice are irradiated, the sooner they develop more severe stages of cataracts in a manner different than the processes in lenses of adult mice. However, questions remain regarding the precise nature of cataracts and their formation in the lens.

The high radiation resistance of the retina of adult FVB x 129/Ola hybrids was demonstrated by Gorgels et al. [2007] with a dose of up to 15 Gy (7.47 Gy/min). Little is known, however, about the retinal reaction of very young mice to IR. Lucas [1961] reported that P4-irradiated mice (CBA/H strain), irradiated with an x-ray dose of 600 rads ($\sim$ 6 Gy), displayed a transient accumulation of pyknotic nuclei in the central space and that a thinner inner and outer nuclear layer of the surviving retinal tissue were discernable 72h after exposure (data was not quantified). Prenatal irradiation of mice has been conducted with subsequent loss of amacrine and ganglion cells [Schmidt et al., 2001]. Borges et al. [2004] investigated the apoptotic response of 129 P1-P3 mice without analysing the layer composition.

In the current study, we demonstrate that cataract formation in neonatal mice after exposure to 2 Gy of low LET IR (γ-rays) is reproducible in other mice (B6C3F1 hybrid strain) and refine the cataract model of Gajewski et al. [1977] (derived from slit-lamp examinations) by an unprecedented combination of the newest *in-vivo* imaging methods, namely optical coherence tomography (OCT) for the detection of the posterior lens and Scheimpflug imaging for the density quantification of the residual lens. Furthermore, we expand knowledge regarding the phenotype of radiation-impaired murine neonatal retinae by quantification and *in-vivo* characterisation.
Finally, we assessed the visual acuity of the mice to understand the long-lasting influences of retinal and lenticular changes on the vision of irradiated neonatal mice.

2. Materials and Supplies

2.1. Mice and irradiation

F1 hybrids of C3HeB/FeJ and C57BL/6JG mice (B6C3F1) were defined as wild types and B6C3F1 mice with a heterozygous point mutation in the *Ercc2* gene (*Ercc2*$^{+/S737P}$) as mutants [Kunze et al., 2015][Dalke et al., 2018]. We exposed mice aged postnatal day 2 (P2) to γ-radiation (Tab. 1) and x-radiation. Twenty mice of each sex and genotype combination (WT♂, WT♀, Mut♂, Mut♀) were exposed to 2 Gy of γ-rays from a ^{60}Co source (Eldorado 78 teletherapy irradiator, Atomic Energy of Canada Limited, Chalk River, Canada). The same number of mice were sham-irradiated. Another six mice of every group were exposed to 2 Gy of x-rays (X-Strahl RS225 irradiator). P2 mice were placed in a Petri dish, covered with a perforated lid to restrict the mice from crawling over each other. Whole-body irradiation by x-rays was applied at a dose rate of 0.367 Gy/min (Cu filter) and at a dose rate of 0.3 Gy per minute for γ-irradiation. Dosimetry was conducted using the UNIDOS II dosimeter (secondary electrometer, calibration was based on the primary standards of the Physikalische-Technische Bundesanstalt-Braunschweig).
Mice were kept under specific pathogen-free conditions at the German Mouse Clinic (GMC, `https://www.mouseclinic.de`) in accordance with the German Law of Animal Protection, the ARVO Statement for the Use of Animals in Ophthalmic and Vision Research, and the tenets of the Declaration of Helsinki. All mice were irradiated and examined with the permission of the Government of Upper Bavaria under ROB-55.2-2532.Vet_02-16-167.

2.2. Scheimpflug imaging and analysis

The lens opacity was analysed using the Scheimpflug system Pentacam® (Oculus GmbH, Wetzlar, Germany) according to the procedure described by [Puk et al., 2009]. Mydriasis was induced by 0.5 % atropine drops to allow optimal visualisation of the lens. Mean and maximum opacities were determined by measuring lenses with the free route tool (to cover the entire lens under exclusion of the corneal reflection point, rather than using the simple line tool).

2.3. OCT and analysis

Optical Coherence Tomography of the lens was performed using the Spectralis® OCT (Heidelberg Engineering, Heidelberg, Germany) as described by Pawliczek et al. [2019]; OCT of the retina was performed according to Puk et al. [2013]. In brief, a 78-diopter double aspheric lens (Volk Optical, Inc.,

Table 1: Mouse cohorts.

Groups	# Mice	Irradiation	Endpoint p.i.
WT (♂/ ♀) + Mut (♂/ ♀)	20	0 Gy	8.5 mths.
WT (♂/ ♀) + Mut (♂/ ♀)	20	2 Gy γ-rays (1.33 MeV)	

Numbers (#) of treated mice of each group (male and female WTs plus male and female mutants) and respective quality of the applied radiation.

Mentor, OH, USA) was directly fixed on the optical outlet of the device. A second plan-convex contact lens (Roland Consult, Brandenburg, Germany) was reversibly attached to the eyes of the mice with contact medium (Methocel 2 %, OmniVision, Puchheim, Germany). The mice were anaesthetised with ketamine (100 mg/kg) and xylazine (10 mg/kg). OCT and Scheimpflug data were deposited in STORE^{DB} (DOI revealed with final version).

2.4. Visual acuity

The optokinetic reflex was determined using an OptoMotry virtual drum system (Cerebral Mechanics, Lethbridge, Canada) [Prusky et al., 2004]. The mice were adapted to room conditions for half an hour before examination. A threshold for vision was determined manually and expressed as spatial frequency (*measure/combine* mode).

2.5. Histological and immunohistochemical analysis

After the mice were sacrificed, the enucleated eyes were fixed in Davidson solution and subsequently embedded in Technovit® 8100 (Heraeus Kulzer, Wehrheim, Germany) after their endpoint (see 1). Samples were cut in 2 µm mid-sagittal sections with a glass knife ultramicrotome (OM U 3, C. Reichert, Austria), heat-fixed on superfrost slides and stained with basic fuchsin and methylene blue. The slides were then scanned using the EVOS® FL Auto Imaging System and the images were processed with an image-processing programme (GIMP 2.8.2, 2017: The GIMP team, `https://www.gimp.org`). Eyes for immunochemical analysis were fixed in 4 % paraformaldehyde for 18 hours after sacrifice. They were then embedded in paraffin and cut in 4 µm sections. Anti-calretinin (Swant, 7699/3H, 1:100), anti-GFAP (Sigma-Aldrich, G926, 1:200), anti-PKCα (abcam, ab-11723, 1:100) and anti-rhodopsin (Santa Cruz, sc-57432, 1:100) were used as antibodies.

The initial OCT investigations of the lens and retina were conducted 2.5, 5.5 and 8.5 months post irradiation (p.i.). Scheimpflug measurements were conducted one time a month beginning 2.5 months p.i.. Finally, mice were examined with the virtual drum 8.5 months p.i. and were subsequently killed for histological and immunohistochemical analysis.

3. Results

3.1. Lenticular alterations

Lenticular OCT. First *in-vivo* measurements of lenses with OCT, conducted 2.5 months p.i., revealed prevalent cortical scattering (Fig. 1, D-F) and nuclear or whole-lens scattering in relatively rare cases (Fig. 1, B). Such alterations of the lens were not recorded in any of the investigated control lens (Fig. 1, A, Tab. 1, controls). Histological analysis of the lenses 8.5 months p.i. identified fringe-like scattering structures in OCT (Fig 2, A) as zones of disordered fibre cells at the interface of the posterior inner cortex and outer nucleus (red arrows). These zones were composed of a sharp edge of possible cell nuclei debris beginning in the cortex and a mixed layer of vacuoles and mispositioned fibre cells, respectively. Based on this comparison, we assigned the fringe scattering patterns as inner cortical cataracts. The more inner parts of the lens were already in the lens region inaccessible for chemical fixation. Therefore, nuclear scattering could not be displayed in histology.

All groups of mice that were exposed to γ-radiation displayed a similar distribution of cataract occurrence in OCT 8.5 months p.i. (Tab. 2). There were almost no lenses without aberration (except in female WT) and only a few nuclear or total cataracts were recorded. The lowest occurrence of cortical cataracts was observed in the female WT and Mut group (87.5 %), whereas the highest occurrence appeared in the male Mut and WT

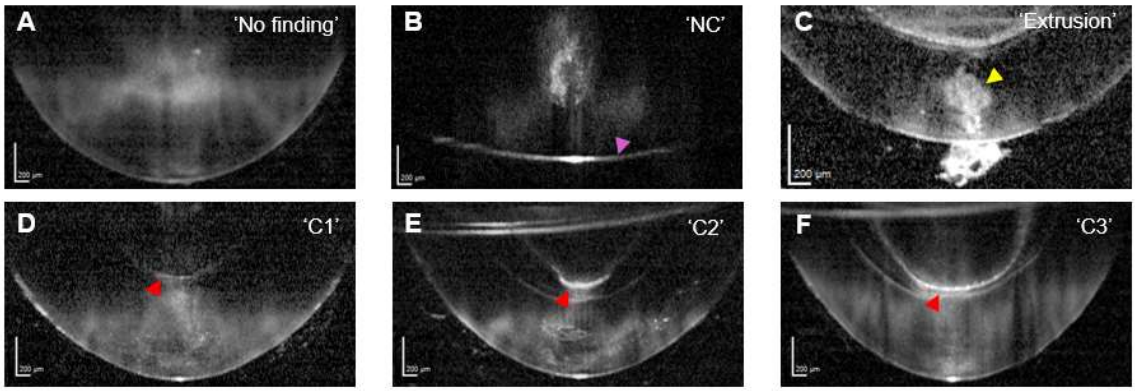

Figure 1: *In-vivo* lens phenotypes based on OCT imaging (**A-E**). No findings (**A**). Nuclear cataract; purple arrowhead indicates interference (**B**). Lenticular extrusion: yellow arrowhead indicates scattering connection between the lesion and extrusion. Please mind increased magnification compared to the other pictures (**C**). Posterior cortical scattering categorised by damage extent; red arrowheads indicate main cortical alterations (**D-F**). Mild type with first appearance of scattering fringe (**D**). Medium type with stronger scattering and first appearance of cleft development (**E**). Severe type with progressed cleft formation (**F**).

Table 2: *In-vivo* OCT pattern frequencies in all γ-irradiated lenses 8.5 months after γ-irradiation.

		Cortical cataract					Phenotype
	Group	**C1**	**C2**	**C3**	**NC/TC**	**No finding**	**symmetry**
Controls	WT ♂	0	0	0	0	34	100 %
	WT ♀	0	0	0	0	36	100 %
	Mut ♂	0	0	0	0	40	100 %
	Mut ♀	0	0	0	0	40	100 %
2 Gy	WT ♂	14	12	11	2	1	85 %
	WT ♀	16	12	7	0	5	72 %
	Mut ♂	9	9	19	2	1	70 %
	Mut ♀	17	10	8	3	2	84 %

Categorisation of affected and not-affected lenses: Mild cortical scattering fringe pattern (**C1**). Medium cortical scattering fringe (**C2**). Severe cortical scattering fringe (**C3**); Subcategories retrievable in Fig. 1., D-F. Nuclear Cataract/Total cataract (**NC/TC**). Exact phenotype symmetry (e.g. C1 cataract or no finding in both lenses) of each animal expressed as percentage of the animals of every cohort.

grouo (92.5 %). Although not drastically different in numbers, the types of cortical cataracts were not equally distributed. Subdivided into 3 levels of severity, mild (C1, Fig. 1, D), medium (C2, Fig. 1, E) and severe (C3, Fig. 1, F), the male mutants developed mainly C3 cortical cataracts (47.5 %) and only 1 lens was not affected at all, compared with 5 in the female WT group. These cortical phenotypes were not stable over the observation time. In several lenses a second scattering fringe appeared in addition to the existent one (Fig. 3, $\Delta t = 3$ months). Because this separation in course of time was highly characteristic for irradiated P2 mice, we named this *in vivo*-detectable feature διάστασις (diastasis). Up to 59 % of the lenses with cortical cataract in mutant male group and only 38 % of the lenses in wilde-type males displayed diastasis. Lenses with severe phenotypes (C2/C3) were more affected than lenses with C1 phenotype. Some lenses with total cataract (5 of 160 irradiated lenses) dissolved over time until only a shrunken remnant of the lens body remained (supplemental data, Fig. 1).

In addition to the enumerated cataract types, several lenses displayed further posterior cortical damage *in vivo* in which lens material was ejected to the vitreous (Fig. 1, C). Those lens extrusions

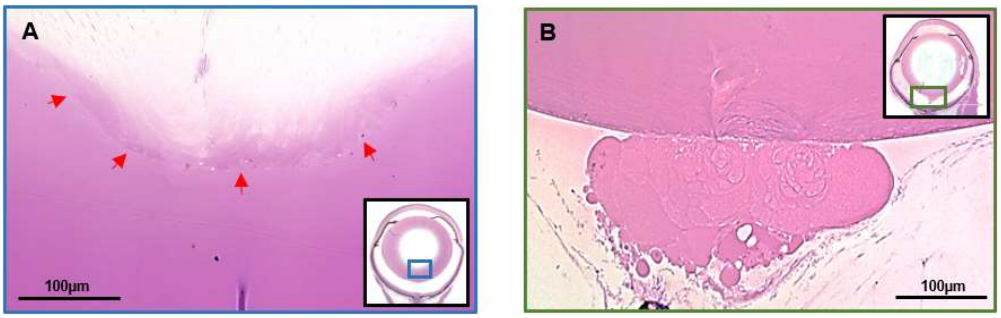

Figure 2: Histology of cortical cataract and lenticular extrusion 8.5 months after exposure. Histological close-up of the lesion in 1, E, magnified 20x (**A**). Red arrows indicate altered lens spots. Histological close-up of lenticular extrusion in 1, C perpendicular to the cortical lesion (**B**). Magnified 40x.

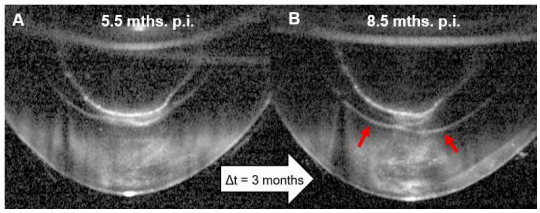

Figure 3: Cataract progression. Representative diastasis example (red arrows indicate fringe separation spots), developing between 5.5 (**A**) and 8.5 months p.i. (**B**).

Table 3: Frequency of diastasis in all groups as a fraction of all lenses with inner cortical cataracts visible in OCT and breakdown of diastasis phenotype on inner cortical cataract type.

Group	C1 (%)	C2 (%)	C3 (%)	Total (%)
WT ♂	0	29.7	8.1	37.8
WT ♀	5.7	25.7	17.1	48.5
Mut ♂	5.4	24.3	29.7	59.4
Mut ♀	14.3	25.7	14.3	55.3

Total fraction is the number of affected lenses divided by number of all lenses of one group investigated.

could be characterised histologically as fibre cells squeezed out by mechanical forces through the lens capsule at small spots in the vicinity of the posterior suture (Fig. 2, B). The bulk of fibre cells in the surrounding region appeared to be not affected in shape and structure. In OCT images of the extrusion, a bolt-like scattering structure crossed the posterior lens coming from the cataractous zone (Fig. 1, C, yellow arrow). It is important to underline that these disruptions of the fibre cell organisation were never observed at more than 1 spot per lens and were not necessarily positioned directly at the suture of the posterior lens but close (see supplemental data for further examples, Fig. 2).

In the cohorts exposed to γ-radiation these extrusions occurred in female WTs and male mutants in every eighth lens (supplemental data, Tab. 1). Controls were also not suspicious for this feature.

Scheimpflug imaging. In a second *in-vivo* approach, we monitored all animals with the Scheimpflug camera. At 8.5 months p.i. only the irradiated mutant groups had significantly higher mean densities than the controls (Fig. 4, A). The mean lens density of male mutants was highest, owing to 2 total cataract outliers. The maximum density was significantly increased in all irradiation cohorts (Fig. 4, B), with the exception of female WT. C3-cortical cataracts at the interface of the nucleus and posterior cortex were confirmed to reach up to the anterior cortex with low-scattering tails (Fig. 4, G). Nuclear cataracts were not accompanied by outer cortical alterations within the observation time (Fig. 4, D). Scheimpflug imaging records substantiated the entirely scattering spot-free OCT images of controls (Fig. 4, C) which is reflected in the steep maximum lens density distributions of all controls.

It is noteworthy that only $\sim$ 50 % of cortical cataracts imaged with OCT were possible to detect with Scheimpflug imaging owing to the closeness of the scattering fringe to the posterior signal boundary.

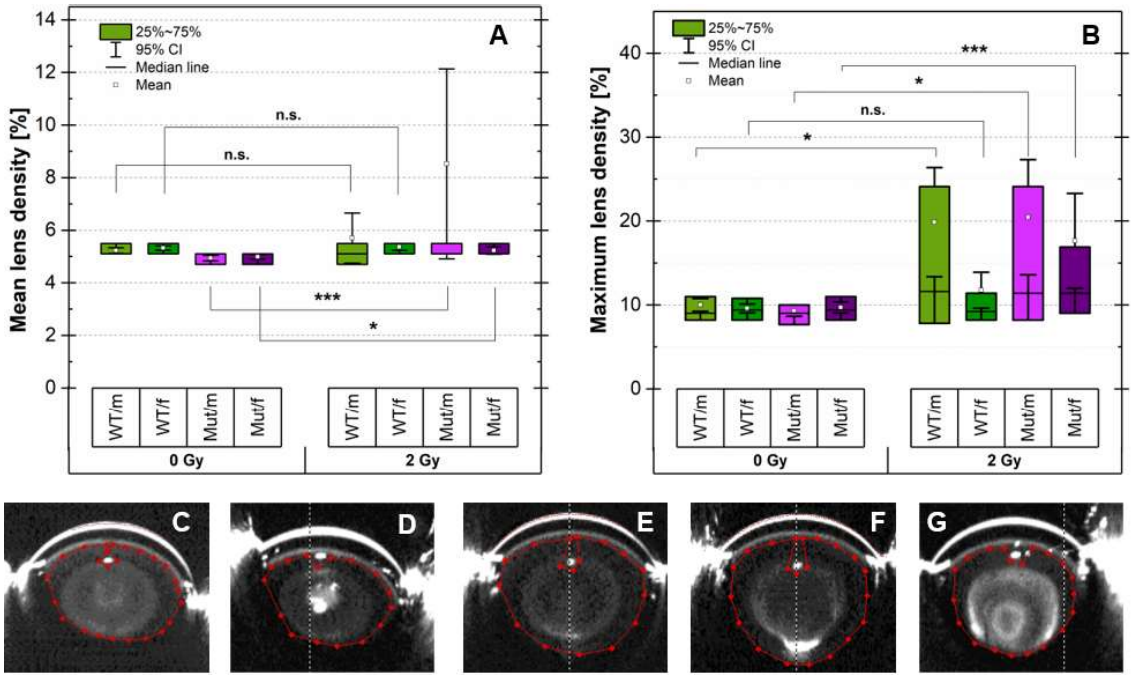

Figure 4: Scheimpflug imaging of the lens 8.5 months after exposure to γ-radiation. Mean lens densities of control and irradiated mice (**A**). Maximum lens densities of control and irradiated mice (**B**). Significances were determined with 2-sided Mann-Withney test. Representative Scheimpflug images of observed phenotypes (**C-G**). Example of a control eye (**C**). Example of a nuclear cataract (**D**). Example of an C1 cortical cataract (**E**). Example of an C2 cortical cataract (**F**). Example of a severe C3 cortical cataract (**G**). Please mind the maximised contrast of the displayed Scheimpflug pictures. Red dots and lines in C-G indicate the area of the measured lens density.

3.2. Retinal alterations

Besides lenticular alterations, massive retinal damage was also observed. The pure thickness of the retina, measured with OCT, was already drastically decreased only 2.5 months p.i. with γ-rays (Fig. 5, A). It was also evident that irradiated retinae shrank over time faster than control retinae which degenerated naturally (Fig. 5, A, comparison between 2.5 and 8.5 months p.i., 5.5 months p.i. omitted for clarity). OCT images for comparison of the control (Fig. 5, C) and irradiated retinae (Fig. 5, D) suggested that the observed shrinking of the thickness of the irradiated retina between 2.5 and 8.5 months p.i. was most likely caused mainly by a massive atrophy of both nuclear layers.

Based on histological analysis, the mean number of outer nuclei was at least quartered (male mutants) or even reduced to one-tenth of the control mean nuclei (male WT) (Fig. 5, B). Therefore, the inner and outer segments were scarce as well.

Besides that, the inner nuclear layer and the outer plexiform layer appeared to be affected, but not the ganglion cell layer or the inner plexiform layer (Fig. 5, F). The inner and outer nuclear layer intermingled at spots of maximum atrophy, whilst control retinae nuclear layers were clearly separated (Fig. 5, E).

Extremely thin retinal spots of irradiated mice appeared in OCT fundus records as round white patches (Fig. 6, B-D, red arrows). These spots were completely deprived of photoreceptors as highlighted in the OCT images of those sections (Fig. 6, B-D, red braces). The appearance of photoreceptor-depleted zones around the optic nerve (ON), first seen 5.5 months p.i. (Fig. 6, E, second row) was very intriguing. The size of the combined lesions surrounding the ON from both eyes of each mouse were expressed as a fraction of the entire measured fundus (ON-surrounding retinal lesions area (ONLA) score, Fig. 6, F). Male WTs appeared to have the most expanded

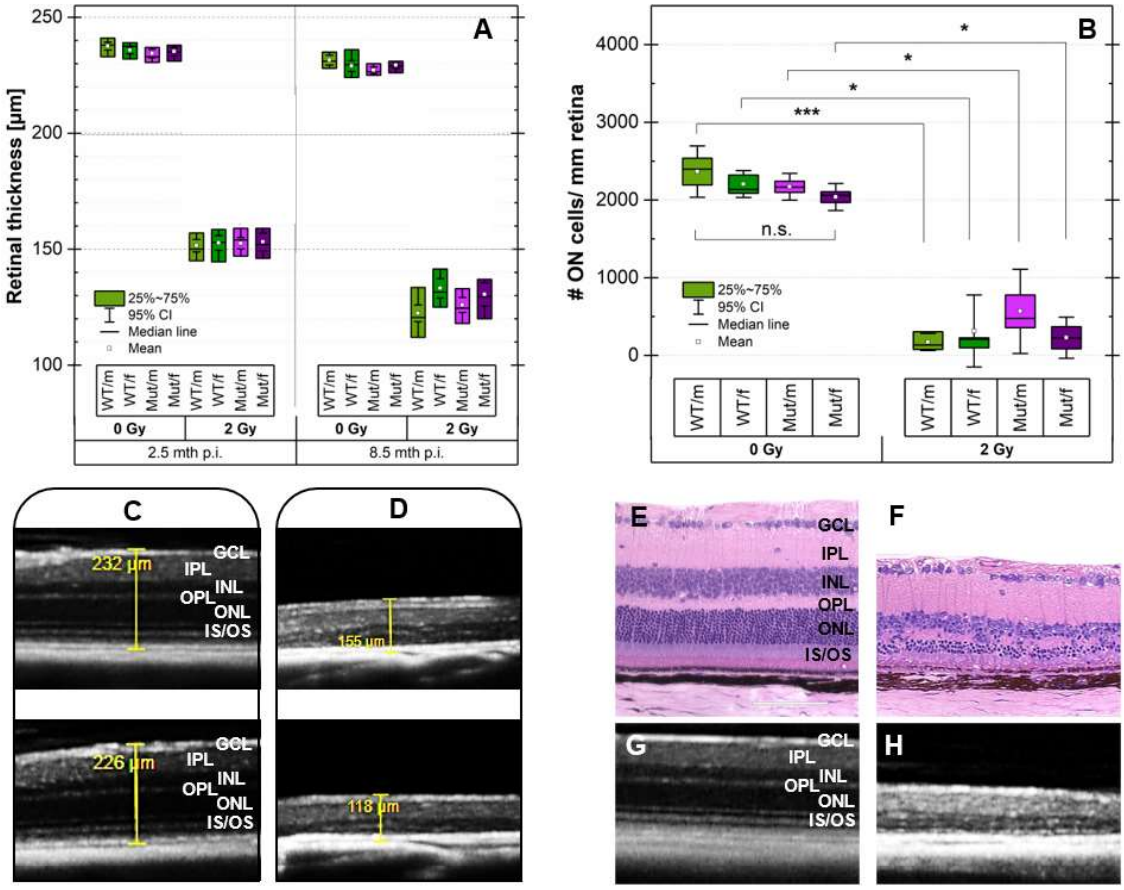

Figure 5: OCT-based measuring of retina and histological analysis. Comparison of *in-vivo* retinal thickness of γ-irradiated mice with controls 8.5 months p.i. (**A**). Outer nuclear layer cell quantity *post mortem* (**B**). Significances determined with 2-sided Mann-Whitney-test. OCT examples for retinal degeneration comparison: Control (**C**) and irradiated example (**D**) with records 2.5 months p.i. (top) and 8.5 months p.i.(bottom). Histology of a male WT control retina (**E**) and of an irradiated retina (**F**) 8.5 months p.i., magnified 20x. Corresponding OCT images of these histology above (**G**+**H**). GCL=Ganglion cell layer, IPL=Inner plexiform layer, INL=Inner nuclear layer, OPL=Outer plexiform layer, ONL=Outer nuclear layer, IS/OS= Inner/Outer segments.

lesions of all irradiated groups. Also, the fraction of eyes displaying any sign of lesions around the ON was highest in males (77.8 % in WTs, 66 % in mutants). Female WTs displayed this phenotype in 51 % of the investigated fundus and 46 % of the female mutants.

Retinal blood vessels of controls rose normally from the optical disc and spread to the retinal periphery (see Fig. 6, A left). This regular pattern disappeared completely in irradiated mice (see Fig. 6, C left). Only short-reaching main vessels could be detected in fundus images; in some samples, no vessel were detected at all.

Thinner inner and outer segment layers recorded *in vivo* by OCT were matched by scarce and irregularly distributed rhodopsin signal in irradiated samples in comparison to controls (Fig. 7, B, example shown for male mutants). More surprisingly, glutathione peroxidase 1 (GPX1) signal was more intense in the remaining photoreceptor cells of irradiated mice (Fig. 7, C) than in photoreceptors of controls.

Horizontal cells labelled with protein kinase C α (PKCα), which is highly expressed in axons and

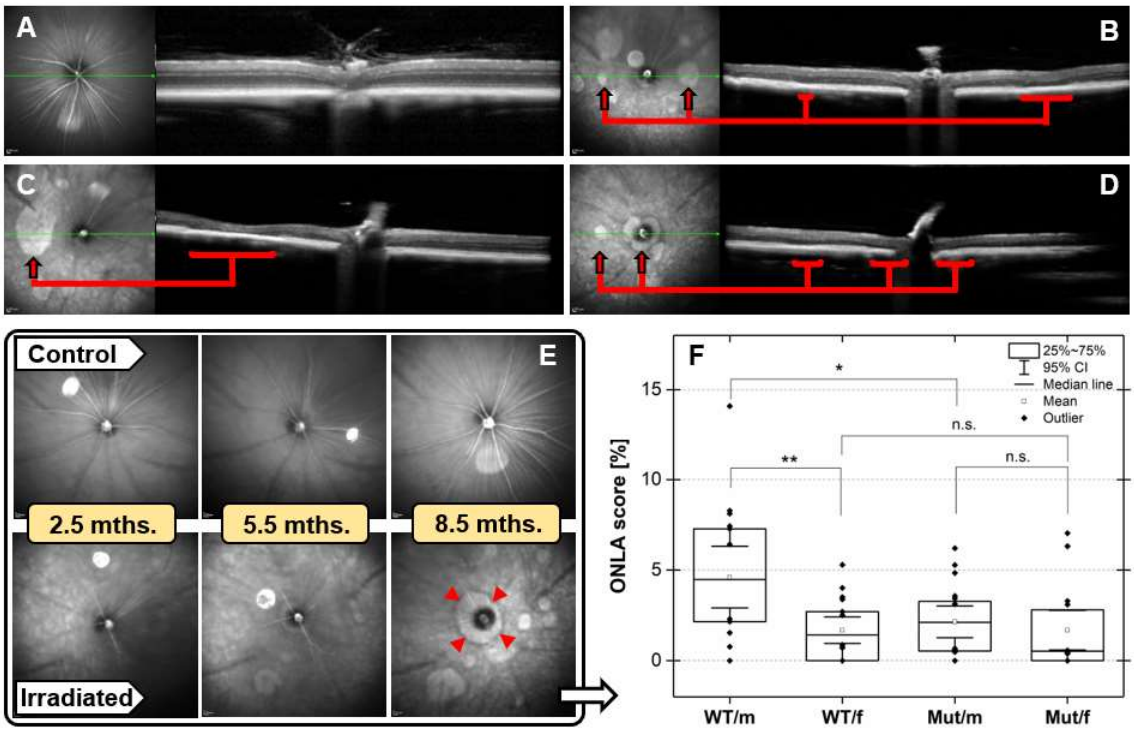

Figure 6: Fundus analysis with representative tomographies of investigated mice 8.5 months p.i.. Control (**A**). Irradiated male Mut with several photoreceptor-depleted areas (**B**). Irradiated female Mut with peripheral lesion (**C**). Irradiated female Mut with concentric photoreceptor-depleted area around the optic nerve (ON) (**D**).Fundus dynamics of a female Mut control (first row) and irradiated male Mut mouse (second row). Comparison between condition 2.5, 5.5 and 8.5 months p.i. (**E**). ONLA (ON-surrounding retinal lesions area) score of each irradiated mouse (**F**). Significances determined with 2-sided Mann-Withney test. Red arrows indicate local dents. Red arrowheads indicate ON-surrounding retinal lesions.

dendrites, were detected in retinae of controls and irradiated mice mainly in the upper inner and the outer plexiform layer without differences (Fig. 8, B). In addition, amacrine cells (upper inner nuclear layer) and ganglion cells (ganglion cell layer) were most likely unchanged in the irradiated retinae. The 3 regularly ordered synaptic connection bands in the inner plexiform layer were present in all irradiated retinae, despite missing photoreceptors (Fig. 8, C).

The atrophy of the neural retina was accompanied by inflammation-related increase in expression of glial fibrillary acidic protein (GFAP) in the ganglion cell layer and in the inner plexiform layer as vertical spikes (Fig. 9, right); a feature not observable in control mice (9, left).

3.3. Visual acuity

The visual acuity of control and γ-irradiated mice was determined 8.5 months p.i.. The measured mean acuity was reduced in all irradiated groups (Fig. 10, A). The lowest reduction occurred in the group of female mutants (45 %, $p < 10^{-7}$) and highest reduction was observed in irradiated male wild types (55 %, $p < 10^{-7}$). Three-way-ANOVA assured that no factors other than dose ($p \rightarrow 0$) influenced the dependent quantity spatial frequency of the investigated mice.

To assess, whether retinal and lenticular damage might correlate with the impairment of visual acuity, combined retinal thickness of both eyes of each animal was plotted against the outcome in the virtual drum. For each animal a cataract score was calculated and added by colour code to each visual acuity result. Surprisingly, neither

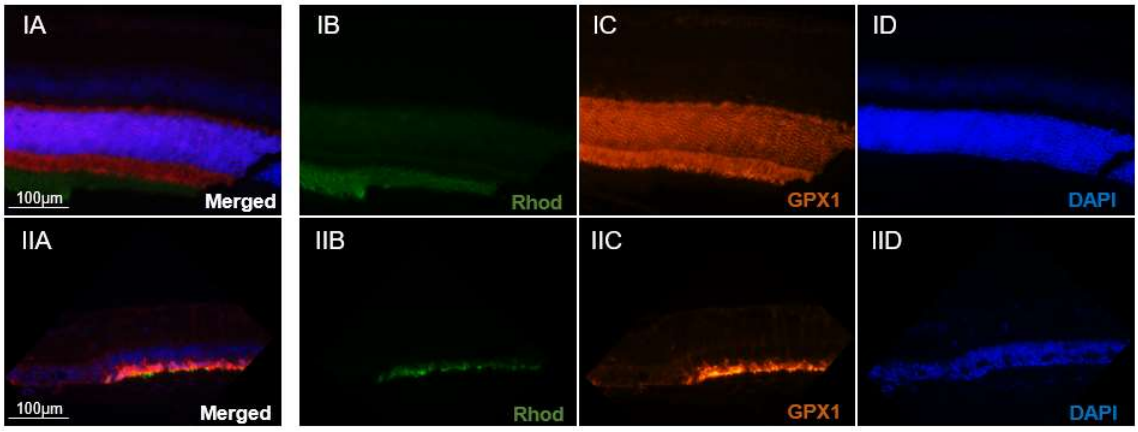

Figure 7: Rhodopsin and GPX1 expression in male mutants 8.5 months after exposure, magnified 20x. Control (**I**) and irradiated sample (**II**). Merged (**A**), rhodopsin (**B**), GPX1 (**C**) and DAPI (**D**).

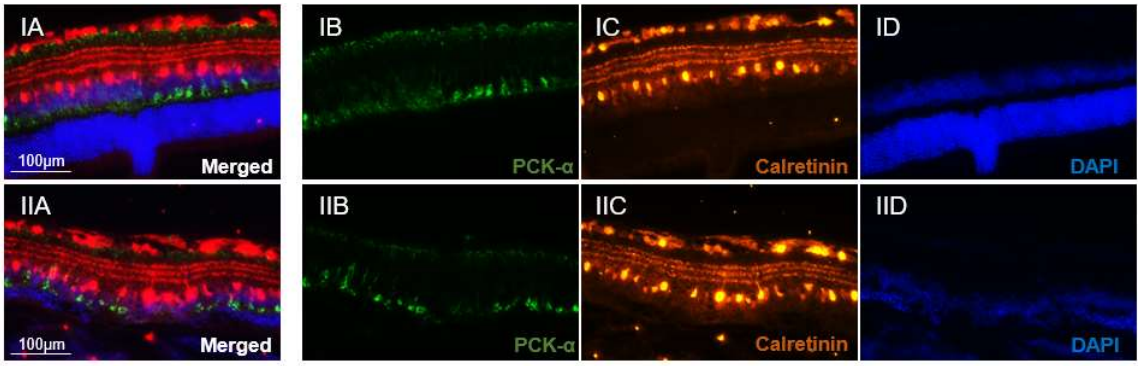

Figure 8: PKCα and calretinin expression in male mutants 8.5 months after exposure, magnified 20x. Control (**I**) and irradiated sample (**II**). Merged (**A**), PKCα (**B**), calretinin (**C**) and DAPI (**D**).

a clear correlation with retinal thickness nor a clear separation by cataract score was recognisable (Fig. 10, B). Several animals with cataractous eyes were relatively less vision-impaired than a subgroup with comparable retinal thickness, but less damaged lenses (lower left diagram region). Based only on the irradiated mice, a solid linear regression was not successful.

4. Discussion

Because boundaries between the categories were fluid (except C1 cortical cataracts), arbitrarily categorized lenticular damage in grades of severity was naturally prone to misjudgement. Still, overall damage distribution was pre-eminent and demanded a rough classification. To categorise the lenticular *in-vivo* phenotypes based on OCT rather than of Scheimpflug imaging was also justified by the better visibility of posterior cortical alterations. OCT monitoring offered valuable insights into the makeup and dynamics of observed cataracts. Fibre cells of a very defined area were affected. Owing to the late beginning of measurements 2.5 months p.i., it continues to be speculation that initial epithelial damage caused by IR was responsible, but the hypothesis can also not be rejected by our data. Specifying the fibre cells as enlarged is substantiated by histology, although the scattering effect in OCT might be caused instead by cell nuclei debris and the overall structural disorder of fibre cells at both sides of the cleft.

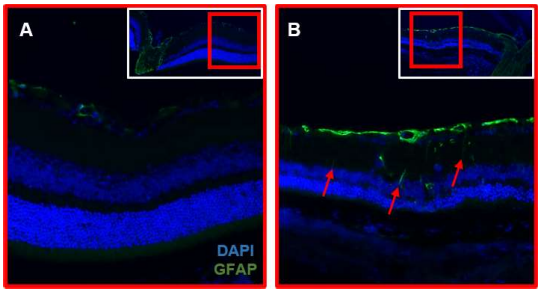

Figure 9: GFAP expression in retinae 8.5 months after exposure to γ-radiation, magnified 20x. Control retina (**A**). Retina of an irradiated mouse (**B**). ← indicate GFAP signal spikes inside the inner plexiform and inner nuclear layer.

It remains unclear, whether diastasis represented a secondary effect in the lens after ∼ 5.5 months or whether the scattering rings appearing posterior the main damage were parts of the initial damage and the space between filled up with regular fibre cells. Phenotype of intersecting wave fronts in diastasis (Fig. 3, B) hardened the suspicion of a secondary effect. In some lenses, the cataracts seemed to lose intensity after diastasis and the space between 2 rings scattering-free. Although this appeared as a mitigation of the lesion, parallel development to nuclear cataract was immanent (see Fig. 4, G). The heterozygous *Ercc2* mutation had a lesion severity-increasing effect only on males, but a diastasis-promoting effect in both sexes.

The nuclear and total cataracts were seen only in irradiated mice (see Tab. 2). Nonetheless, it is highly doubtful that nuclear scattering as in Fig. 1 B was caused by IR because primary fibre cells were formed before P2. Overall the odds ratio of a nuclear and total scattering in lenses of irradiated mice compared to controls was 15.6 but was not significant ($p = 0.06$).

A posterior subcapsular cataract was observed in only in 1 lens in addition to the inner cortical cataract 8.5 months p.i. (see supplemental data, Fig. 3). This was not surprising, because alterations at the posterior pole are a distinguished feature of mice irradiated several weeks after birth [Gajewski et al., 1977]. It cannot be excluded that PSCs could have been observed more than 8.5 months p.i.. Anterior alterations were also not observed (based on Scheimpflug imaging).

Scheimpflug imaging delivered important complementary information. Despite obvious local lesions, the median of mean densities was significantly higher only in mutants than in controls. Speaking in terms of the lens opacities classification system III criterium for a human nuclear cataract type 2 (mean density of 14,4 % or more), all irradiated mice were far from a clinically relevant opacification [Pei et al., 2008]. Even taking into account the low cataract covering of ∼ 50 %, the expectation would have been that the overall density would be higher. That might be an interesting puzzle piece in elucidating the mechanism of IR interaction with the lens. Most likely, some epithelial cells differentiated erroneously and some fibre cells lost their integrity, respectively. Other than that, IR had little effect on most of the primary nuclear fibre cells.

The P2 mice that were irradiated with 2 Gy of x-rays exhibited a similar pattern in cortical cataract development. No lens was unaffected or developed a nuclear cataract (data not shown).

Overall, the mice in our study showed a comparable cataract incidence to that reported by Gajewski et al. [1977] (all WT 85 % vs 96.7 %) and a much higher incidence than that reported by De Stefano et al. [2015] (all WT 85 % vs 10.18 %). These discrepancies could be explained by different strain radiosensitivity. In addition, the 3 different forms of cataract identification and assessment might have had a significant influence (slit-lamp vs stereomicroscope vs OCT).

Retinal alterations following exposure to γ-rays were less open to interpretation. Overall thickness, measured undistorted and reliably with OCT, was drastically reduced and no data distribution overlap whatsoever occurred (also in x-ray-exposed animals, not shown). Control retinae atrophy was observed as a natural effect, but that irradiated retinae shrank faster than the controls could be deduced to be the result of detrimental long-lasting effects of the radiation on photoreceptor cells. More dispersed thickness distributions of the irradiated retinae 8.5 months p.i. reflected a variant impact of IR on the entire retinae (standard deviation in all irradiated groups ∼ 10 % of the mean retinal thickness).

Most of the retinal layers are not yet differentiated in B6C3F1 mice at P2 (see supplemental data, Fig. 4). It is therefore fair to say that photoreceptor cells at P2 did not develop properly in the aftermath of irradiation, but rather degenerated.

It was also evident that short main vessels, visible

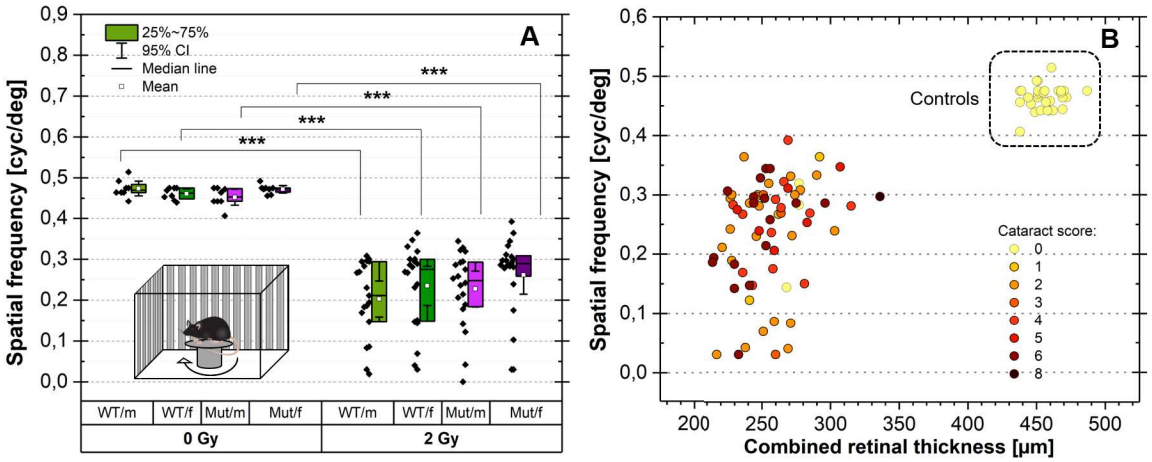

Figure 10: Visual acuity test and correlation with observed damage. Visual acuity of γ-irradiated mice compared with controls 8.5 months p.i. (**A**). Correlation between combined retinal damage (both eyes) and visual acuity (**B**). Cataract scores calculated by addition of values for both eyes. (no findings = 0, C1 = 1, C2 = 2, C3 = 3, small nuclear cataract = 4, total cataract = 5). Significances were determined with Mann-Withney test.

on the fundus, were not necessarily matched by a total degeneration of the photoreceptor layer in the retinal periphery. Paradoxically, ON-surrounding photoreceptor depletion, the patches of maximum atrophy, occurred in many examples first.

GFAP expression in our γ-irradiated mice matched the expression pattern of Sprague-Dawley rats constantly irradiated with visible light for 3 days [Eisenfeld et al., 1984]. In the cited study, GFAP spikes also pervaded the neuroretina, following the specific degeneration of photoreceptors only. Altogether, GFAP expression advocated a reactive gliosis as known from non-regenerating retinal tissue [Dyer and Cepko, 2000]. The enhanced radiation-related expression of GPX1 in photoreceptor cells was not reported before and documented the radiation-induced expression change of a key antioxidant enzyme.

Visual acuity was determined 'manually' which might have influenced the outcome of spatial frequency of some animals. Despite this possible error source, it remained obvious that a simple linear relationship between retinal thickness and spatial frequency was not given. However, even if taking the ONLA-score (central blindness) and cataract score into account, the same conclusion has to be made, namely that the impairment at hand did not sufficiently explain the vision impairment for every mouse. Although it is likely that the combination of cataracts and retinal dysfunction caused the vision impairment of irradiated mice, we cannot exclude other variables such as neuropathological effects of IR on the visual cortex or other relevant centre for vision processing.

Nonetheless, it appeared, that the visual acuity of the 4 irradiated groups as a whole mirrored the results of the ONLA-score (the higher the score, the more probable a central vision deficiency). This also means that retinal damage might outweigh lenticular damage.

5. Conclusion

We demonstrated in this study the deteriorating effects of low LET IR on the optical lens and the retina of neonatal mice. Lens alterations caused by irradiation were monitored *in vivo* and categorised in detail for the first time. All lens phenotypes were radiation-induced and supported the age-dependent typing of Gajewski et al. [1977], but rebutted the observation of 'opaque strands running from the periphery', insofar as we observed only central cortical opacification (type II cataracts in 10-week-old adults after exposure to 2 Gy confirmed, unpublished data). Irradiated retinae proved to be far more sensitive than retinae of adult mice (compared with [Gorgels et al., 2007]) and it is very likely that even lower doses of IR might have had a similar impact. We also

achieved a comprehensive description of retinal changes in P2 mice for the first time and revealed the combined effect of irradiation damages in the eye on murine vision.

Although the transfer of murine experimental data to humans is debatable, it could be concluded that our results shed light on the rather unclear question of how human foetal eyes cope with radiation-enriched environment within their ontogenesis. This applies to pregnant women undergoing radiation therapy (with possible high doses of scattering radiation) and, in the long run, to reproducing populations in the coming age of extraterrestrial settlements and space exploration (γ-ray bursts within the time of the critical developmental corridor). The fact that almost every irradiated mouse was hampered in visual acuity, but that none developed cancer, demonstrated that a vision health agenda should be a top priority in radiation protection in general and in space research in particular. Therefore, more scientific contributions for a mechanistic understanding of the lenticular and retinal alterations are needed, as well as for the deleterious effects of high LET radiation exposure [Hamada and Sato, 2016].

Acknowledgements

We thank Erika Bürkle and Monika Stadler for the excellent technical assistance and Dr. Elizabeth Ainsbury for valuable advice.
The German Mouse Clinic received funding by the German Federal Ministry of Education and Research (Infrafrontier grant 01KX1012 to MHdA).
This study was financed by the LDLensRad project, which received funding from the Euratom Research and Training Programme 2014-2018 under grant agreement No 662287. This publication reflects only the authors' view. Responsibility for the information and views expressed therein lies entirely with the authors. The European Commission is not responsible for any use that may be made of the information it contains.

Disclosure statement

The authors declare to have no potential conflicts of interest.

References

Ainsbury, E.A., Barnard, S., Bright, S., Dalke, C., Jarrin, M., Kunze, S., Tanner, R., Dynlacht, J.R., Quinlan, R.A., Graw, J., et al., 2016. Ionizing radiation induced cataracts: recent biological and mechanistic developments and perspectives for future research. Mutation Research/Reviews in Mutation Research 770, 238–261. doi:10.1016/j.mrrev.2016.07.010.

Borges, H., Chao, C., Xu, Y., Linden, R., Wang, J., 2004. Radiation-induced apoptosis in developing mouse retina exhibits dose-dependent requirement for atm phosphorylation of p53. Cell Death & Differentiation 11, 494. doi:10.1038/sj.cdd.4401366.

Dalke, C., Neff, F., Bains, S.K., Bright, S., Lord, D., Graw, J., Reitmeir, P., Rößler, U., Samaga, D., Unger, K., Braselmann, H., et al., 2018. Lifetime study in mice after acute low-dose ionizing radiation: a multifactorial study with special focus on cataract risk. Radiat Environ Biophys. 57, 99–113. doi:10.1007/s00411-017-0728-z.

De Stefano, I., Tanno, B., Giardullo, P., Leonardi, S., Pasquali, E., Antonelli, F., Tanori, M., Casciati, A., Pazzaglia, S., Saran, A., et al., 2015. The patched 1 tumor-suppressor gene protects the mouse lens from spontaneous and radiation-induced cataract. The American journal of pathology 185, 85–95. doi:10.1016/j.ajpath.2014.09.019.

Diedrichs-Möhring, M., Leban, J., Strobl, S., Obermayr, F., Wildner, G., 2015. A new small molecule for treating inflammation and chorioretinal neovascularization in relapsing-remitting and chronic experimental autoimmune uveitis. Investigative ophthalmology & visual science 56, 1147–1157. doi:10.1167/iovs.14-15518.

Dyer, M.A., Cepko, C.L., 2000. Control of müller glial cell proliferation and activation following retinal injury. Nature neuroscience 3, 873–880.

Eisenfeld, A.J., Bunt-Milam, A., Sarthy, P.V., 1984. Müller cell expression of glial fibrillary acidic protein after genetic and experimental photoreceptor degeneration in the rat retina. Investigative ophthalmology & visual science 25, 1321–1328.

Gajewski, A., Majewska, K., Słowikowska, M., Chomiczewski, K., Kulig, A., 1977. Types and rate of cataract development in mice irradiated at different ages. Radiation research 71, 471–480.

Gorgels, T.G., van der Pluijm, I., Brandt, R.M., Garinis, G.A., van Steeg, H., van den Aardweg, G., Jansen, G.H., Ruijter, J.M., Bergen, A.A., van Norren, D., et al., 2007. Retinal degeneration and ionizing radiation hypersensitivity in a mouse model for cockayne syndrome. Molecular and cellular biology 27, 1433–1441. doi:10.1128/MCB.01037-06.

Hamada, N., Sato, T., 2016. Cataractogenesis following high-let radiation exposure. Mutation Research/Reviews in Mutation Research 770, 262–291. doi:10.1016/j.mrrev.2016.08.005.

Kleiman, N.J., 2012. Radiation cataract. Annals of the ICRP 41, 80–97. doi:10.1016/j.icrp.2012.06.018.

Kunze, S., Dalke, C., Fuchs, H., Klaften, M., Rössler, U., Hornhardt, S., Gomolka, M., Puk, O., Sabrautzki, S., Kulka, U., et al., 2015. New mutation in the mouse *Xpd/Ercc2* gene leads to recessive cataracts. PLoS One. 10, e0125304. doi:10.1371/journal.pone.0125304.

Lucas, D., 1961. The effect of x-radiation on the mouse retina at different stages of development. International

Journal of Radiation Biology and Related Studies in Physics, Chemistry and Medicine 3, 105–124. doi:10.1080/09553006114550131.

Ohlmann, A., Scholz, M., Goldwich, A., Chauhan, B.K., Hudl, K., Ohlmann, A.V., Zrenner, E., Berger, W., Cvekl, A., Seeliger, M.W., et al., 2005. Ectopic norrin induces growth of ocular capillaries and restores normal retinal angiogenesis in norrie disease mutant mice. Journal of Neuroscience 25, 1701–1710. doi:10.1523/JNEUROSCI.4756-04.2005.

Pawliczek, D., Dalke, C., Fuchs, H., Gailus-Durner, V., de Angelis, M.H., Graw, J., Amarie, O.V., 2019. Spectral domain-optical coherence tomography (sd-oct) as a monitoring tool for alterations in mouse lenses. Experimental Eye Research , 107871doi:10.1016/j.exer.2019.107871.

Pei, X., Bao, Y., Chen, Y., Li, X., 2008. Correlation of lens density measured using the pentacam scheimpflug system with the lens opacities classification system iii grading score and visual acuity in age-related nuclear cataract. British Journal of Ophthalmology 92, 1471–1475. doi:10.1136/bjo.2007.136978.

Prusky, G.T., Alam, N.M., Beekman, S., Douglas, R.M., 2004. Rapid quantification of adult and developing mouse spatial vision using a virtual optomotor system. Investigative ophthalmology & visual science 45, 4611–4616. doi:10.1167/iovs.04-0541.

Puk, O., Hrabě de Angelis, M., Graw, J., 2013. Longitudinal fundus and retinal studies with SD-OCT: a comparison of five mouse inbred strains. Mamm Genome. 24, 198–205. doi:10.1007/s00335-013-9457-z.

Puk, O., Dalke, C., Calzada-Wack, J., Ahmad, N., Klaften, M., Wagner, S., Hrabě de Angelis, M., Graw, J., 2009. Reduced corneal thickness and enlarged anterior chamber in a novel ColVIIIa2G257D mutant mouse. Invest Ophthalmol Vis Sci. 50, 5653–5661. doi:10.1167/iovs.09-3550.

Schmidt, S.L., Vitral, R.W., Linden, R., 2001. Effects of prenatal ionizing irradiation on the development of the ganglion cell layer of the mouse retina. International Journal of Developmental Neuroscience 19, 469–473. doi:10.1016/S0736-5748(00)00068-X.

Uwineza, A., Kalligeraki, A.A., Hamada, N., Jarrin, M., Quinlan, R.A., 2019. Cataractogenic load–a concept to study the contribution of ionizing radiation to accelerated aging in the eye lens. Mutation Research/Reviews in Mutation Research doi:10.1016/j.mrrev.2019.02.004.

Review Report 11 December 2020

We thank the reviewer for accurately reading of the manuscript and the comments. Our answer are given below in *italic.*

Reviewer #1: The revised manuscript submitted in a carefree action, with no figure numbers and table numbers has challenged the review. In addition, not submitted references are in the manuscript text "blinded" and the supplementary material was not possible to open. These all make it not pleasant to align text to figures, tables and missing supplementary data, I hope will give proper care to all these misses at the final submission.
The authors improved some of the suggested points in the manuscript, but the difficultly to read their lines still persists, often sentences need to be red again to get the point.

We are honestly puzzled about this. We delivered a pdf file with the usual labelling of tables and figures and additionally submitted the figures as png files. The manuscript pdf file was intact and the figures were in proper form when we checked it. Therefore, we struggle to respond to the comments in this passage. Indeed, the pdf of the supplement was missing, and we send only the labelled figures. That was our fault.

Comments:
- Lane 298: authors state that with OCT the reduced retinal thickness is due to a general atrophy of all layers (did the authors measured each individual layer), but a few lanes down, lanes 305-306 the histology analysis reveal that the IPL and GCL thicknesses are not changed. Does this mean that the OCT is not reliable to pick-up these changes? I think the authors can put this entire part better in words. That part is confusing. As well lanes 310-311 where the authors wrote "retinal pigmented epithelium appeared also perforated".. also like what else? But mostly, do the authors saw/proved that it is a perforation? How does is look like, can we see it, where?

A very good point, thank you for this. We did not measure the thickness of the IPL or GCL, neither in OCT, nor in histology. Point measurements of the thickness would have been very error-prone as you can imagine by the irregular appearance of the retinae. By pure comparison of OCT images and histological sections, the IPL and GCL were almost not affected in thickness. Our general statement in lane 298, all layers seemed to be affected was therefore quite rigorous and speculative respectively and was changed accordingly including the visible alterations: "... was most likely caused mainly by a massive atrophy of both nuclear layers.". The sentence of RPE perforation was crossed out. Indeed, this was a mere speculation.

- Lane 344: "exemplary" is it meant example?

No, the adverb was indented, but we changed it.

- Lane 356: substitute unabatedly with unchanged to make it easier to read. Many of the readers will not have English as native language, and they will all have to look after the meaning of unabatedly and so lose focus on the message emitted (searching unabatedly in PubMed, it comes up in 15 papers, unchanged comes up in 150.121 papers; bottom line: a scientific wording is proper here).

We changed "unabatedly" to "unchanged", although this was an explicit correction of a native speaker. The sentence is now: "In addition, amacrine cells (upper inner nuclear layer) and ganglion cells (ganglion cell layer) were most likely unchanged in the irradiated retinae."

- Lane 357: all irradiated mice "were" is maybe where; here too, the sentence gives you place for own interpretation.

The sentence was changed to "The 3 regularly ordered synaptic connection bands in the inner plexiform layer were present in all irradiated retinae, despite missing photoreceptors (Fig. 8, C).", in order to avoid any missunderstandigs.

- Lanes 464-466: do the authors refer to the nuclear cataract here, to be induced by irradiation?

Not necessarily a nuclear cataract of clinical importance, but a measurable increase of opacification. We changed the sentence anyway to "Other than that, IR had little effect on most of the primary nuclear fibre cells."

- Lanes 467-470: are the x-rays irradiated mice showing also "no finding at all" in their lenses or in the retina, and why there is no finding, as opposite to the previous data provided ?

Again, a lapsus we could have avoided. All the irradiated lenses were affected and formed a cortical cataract of the C1-, C2- or C3-type. There was no lens with a nuclear cataract or without being affected. We changed the sentence for more clarity: "The P2 mice that were irradiated with 2 Gy of x-rays exhibited a similar pattern in cortical cataract development. No lens was unaffected or developed a nuclear cataract (data not shown)." We also included a statement concerning the x-ray effects on the retinae in lane 486. The sentence is now "Retinal alterations following exposure to gamma-rays were less open to interpretation. Overall thickness, measured undistorted and reliably with OCT, was drastically reduced and no data distribution overlap whatsoever occurred (also in x-ray-exposed animals, not shown)."

Highlights

- Ionizing radiation causes cortical cataracts and retinal dysplasia in neonatal mice
- Optical coherence tomography as monitoring tool for posterior cataracts
- Imaging of cortical cataract revealed changing scattering properties
- First revealed lens extrusions after exposure to a moderate dose of ionizing radiation
- Whole-body irradiation impairs visual acuity of neonatal mice

Click here to access/download
Supplementary Material
Supplement1.png

Supplementary Material as tex file

Supplements as pdf file

```
This is pdfTeX, Version 3.14159265-2.6-1.40.21 (TeX Live 2020/W32TeX)
(preloaded format=pdflatex 2020.5.12)  11 DEC 2020 11:38
entering extended mode
 restricted \write18 enabled.
 %&-line parsing enabled.
**manuscript_20201211.tex
(./Manuscript_20201211.tex
LaTeX2e <2020-02-02> patch level 5
L3 programming layer <2020-05-05> (c:/TeXLive/texmf-
local/tex/latex/aries/elsar
ticle.cls
Document Class: elsarticle 2008/10/09, 1.0.2: Elsevier Science
\@bls=\dimen134
(c:/TeXLive/2020/texmf-dist/tex/latex/base/article.cls
Document Class: article 2019/12/20 v1.4l Standard LaTeX document class
(c:/TeXLive/2020/texmf-dist/tex/latex/base/size10.clo
File: size10.clo 2019/12/20 v1.4l Standard LaTeX file (size option)
)
\c@part=\count167
\c@section=\count168
\c@subsection=\count169
\c@subsubsection=\count170
\c@paragraph=\count171
\c@subparagraph=\count172
\c@figure=\count173
\c@table=\count174
\abovecaptionskip=\skip47
\belowcaptionskip=\skip48
\bibindent=\dimen135
) (c:/TeXLive/2020/texmf-dist/tex/latex/graphics/graphicx.sty
Package: graphicx 2019/11/30 v1.2a Enhanced LaTeX Graphics (DPC,SPQR)
(c:/TeXLive/2020/texmf-dist/tex/latex/graphics/keyval.sty
Package: keyval 2014/10/28 v1.15 key=value parser (DPC)
\KV@toks@=\toks15
) (c:/TeXLive/2020/texmf-dist/tex/latex/graphics/graphics.sty
Package: graphics 2019/11/30 v1.4a Standard LaTeX Graphics (DPC,SPQR)
(c:/TeXLive/2020/texmf-dist/tex/latex/graphics/trig.sty
Package: trig 2016/01/03 v1.10 sin cos tan (DPC)
) (c:/TeXLive/2020/texmf-dist/tex/latex/graphics-cfg/graphics.cfg
File: graphics.cfg 2016/06/04 v1.11 sample graphics configuration
)
Package graphics Info: Driver file: pdftex.def on input line 105.
(c:/TeXLive/2020/texmf-dist/tex/latex/graphics-def/pdftex.def
File: pdftex.def 2018/01/08 v1.0l Graphics/color driver for pdftex
))
\Gin@req@height=\dimen136
\Gin@req@width=\dimen137
) (c:/TeXLive/2020/texmf-dist/tex/latex/psnfss/pifont.sty
Package: pifont 2020/03/25 PSNFSS-v9.3 Pi font support (SPQR)
LaTeX Font Info:    Trying to load font information for U+pzd on input
line 63.

(c:/TeXLive/2020/texmf-dist/tex/latex/psnfss/upzd.fd
File: upzd.fd 2001/06/04 font definitions for U/pzd.
```

```
)
LaTeX Font Info:    Trying to load font information for U+psy on input
line 64.

(c:/TeXLive/2020/texmf-dist/tex/latex/psnfss/upsy.fd
File: upsy.fd 2001/06/04 font definitions for U/psy.
))
\c@tnote=\count175
\c@fnote=\count176
\c@cnote=\count177
\c@ead=\count178
\c@author=\count179
\@eadauthor=\toks16
\c@affn=\count180
\absbox=\box45
\keybox=\box46
\Columnwidth=\dimen138
\space@left=\dimen139
\els@boxa=\box47
\els@boxb=\box48
\leftMargin=\dimen140
\@enLab=\toks17
\@sep=\skip49
\@@sep=\skip50
(./Manuscript_20201211.spl) (c:/TeXLive/2020/texmf-
dist/tex/latex/natbib/natbib
.sty
Package: natbib 2010/09/13 8.31b (PWD, AO)
\bibhang=\skip51
\bibsep=\skip52
LaTeX Info: Redefining \cite on input line 694.
\c@NAT@ctr=\count181
)
\splwrite=\write3
\openout3 = `Manuscript_20201211.spl'.

(c:/TeXLive/2020/texmf-dist/tex/latex/geometry/geometry.sty
Package: geometry 2020/01/02 v5.9 Page Geometry
(c:/TeXLive/2020/texmf-dist/tex/generic/iftex/ifvtex.sty
Package: ifvtex 2019/10/25 v1.7 ifvtex legacy package. Use iftex instead.
(c:/TeXLive/2020/texmf-dist/tex/generic/iftex/iftex.sty
Package: iftex 2020/03/06 v1.0d TeX engine tests
))
\Gm@cnth=\count182
\Gm@cntv=\count183
\c@Gm@tempcnt=\count184
\Gm@bindingoffset=\dimen141
\Gm@wd@mp=\dimen142
\Gm@odd@mp=\dimen143
\Gm@even@mp=\dimen144
\Gm@layoutwidth=\dimen145
\Gm@layoutheight=\dimen146
\Gm@layouthoffset=\dimen147
\Gm@layoutvoffset=\dimen148
```

```
\Gm@dimlist=\toks18
) (c:/TeXLive/2020/texmf-dist/tex/latex/base/fleqn.clo
File: fleqn.clo 2016/12/29 v1.2b Standard LaTeX option (flush left
equations)
\mathindent=\dimen149
Applying: [2015/01/01] Make \[ robust on input line 50.
LaTeX Info: Redefining \[ on input line 51.
Already applied: [0000/00/00] Make \[ robust on input line 62.
Applying: [2015/01/01] Make \] robust on input line 74.
LaTeX Info: Redefining \] on input line 75.
Already applied: [0000/00/00] Make \] robust on input line 83.
)) (c:/TeXLive/2020/texmf-dist/tex/generic/babel/babel.sty
Package: babel 2020/04/28 3.43 The Babel package
(c:/TeXLive/2020/texmf-dist/tex/generic/babel/babel.def
File: babel.def 2020/04/28 3.43 Babel common definitions
\babel@savecnt=\count185
\U@D=\dimen150
(c:/TeXLive/2020/texmf-dist/tex/generic/babel/txtbabel.def)
\bbl@readstream=\read2
)
\bbl@dirlevel=\count186
(c:/TeXLive/2020/texmf-dist/tex/latex/ibycus-babel/ibycus.ldf
Language: ibycus 2005/11/23 v3.0 (PH/WaS)
Loading the definitions for the Greek font encoding LGI
(c:/TeXLive/2020/texmf-
dist/tex/latex/ibycus-babel/lgienc.def
File: lgienc.def 2005/11/23 v3.0 (PH/WaS)
Now handling font encoding LGI ...
... no UTF-8 mapping file for font encoding LGI
)) (c:/TeXLive/2020/texmf-dist/tex/generic/babel-german/ngerman.ldf
Language: ngerman 2018/12/08 v2.11 German support for babel (post-1996
orthogra
phy)
(c:/TeXLive/2020/texmf-dist/tex/generic/babel-german/ngermanb.ldf
Language: ngermanb 2018/12/08 v2.11 German support for babel (post-1996
orthogr
aphy)
Package babel Info: Making " an active character on input line 121.
)) (c:/TeXLive/2020/texmf-dist/tex/generic/babel-english/english.ldf
Language: english 2017/06/06 v3.3r English support from the babel system
Package babel Info: \l@canadian = using hyphenrules for english
(babel)             (\language0) on input line 102.
Package babel Info: \l@australian = using hyphenrules for ukenglish
(babel)             (\language21) on input line 105.
Package babel Info: \l@newzealand = using hyphenrules for ukenglish
(babel)             (\language21) on input line 108.
)) (c:/TeXLive/2020/texmf-dist/tex/latex/base/inputenc.sty
Package: inputenc 2018/08/11 v1.3c Input encoding file
\inpenc@prehook=\toks19
\inpenc@posthook=\toks20
(c:/TeXLive/2020/texmf-dist/tex/latex/base/ansinew.def
File: ansinew.def 2018/08/11 v1.3c Input encoding file
)) (c:/TeXLive/2020/texmf-dist/tex/latex/multirow/multirow.sty
Package: multirow 2019/05/31 v2.5 Span multiple rows of a table
```

```
\multirow@colwidth=\skip53
\multirow@cntb=\count187
\multirow@dima=\skip54
\bigstrutjot=\dimen151
) (c:/TeXLive/2020/texmf-dist/tex/latex/multirow/bigdelim.sty
Package: bigdelim 2019/05/31 v2.5 Create big delimiters in tabular or
array
) (c:/TeXLive/texmf-local/tex/latex/aries/subfig.sty
Package: subfig 2005/06/28 ver: 1.3 subfig package
(c:/TeXLive/2020/texmf-dist/tex/latex/caption/caption.sty
Package: caption 2020/01/03 v3.4h Customizing captions (AR)
(c:/TeXLive/2020/texmf-dist/tex/latex/caption/caption3.sty
Package: caption3 2020/01/03 v1.8h caption3 kernel (AR)
Package caption3 Info: TeX engine: e-TeX on input line 61.
\captionmargin=\dimen152
\captionmargin@=\dimen153
\captionwidth=\dimen154
\caption@tempdima=\dimen155
\caption@indent=\dimen156
\caption@parindent=\dimen157
\caption@hangindent=\dimen158
Package caption Info: elsarticle document class detected.
)
\c@caption@flags=\count188
\c@continuedfloat=\count189
)
\c@KVtest=\count190
\sf@farskip=\skip55
\sf@captopadj=\dimen159
\sf@capskip=\skip56
\sf@nearskip=\skip57
\c@subfigure=\count191
\c@subfigure@save=\count192
\c@lofdepth=\count193
\c@subtable=\count194
\c@subtable@save=\count195
\c@lotdepth=\count196
\sf@top=\skip58
\sf@bottom=\skip59
) (c:/TeXLive/2020/texmf-dist/tex/latex/lineno/lineno.sty
Package: lineno 2005/11/02 line numbers on paragraphs v4.41
\linenopenalty=\count197
\output=\toks21
\linenoprevgraf=\count198
\linenumbersep=\dimen160
\linenumberwidth=\dimen161
\c@linenumber=\count199
\c@pagewiselinenumber=\count266
\c@LN@truepage=\count267
\c@internallinenumber=\count268
\c@internallinenumbers=\count269
\quotelinenumbersep=\dimen162
\bframerule=\dimen163
\bframesep=\dimen164
```

```
\bframebox=\box49
LaTeX Info: Redefining \\ on input line 3056.
) (c:/TeXLive/2020/texmf-dist/tex/latex/base/textcomp.sty
Package: textcomp 2020/02/02 v2.0n Standard LaTeX package
) (c:/TeXLive/2020/texmf-dist/tex/latex/pdflscape/pdflscape.sty
Package: pdflscape 2019/12/05 v0.12 Display of landscape pages in PDF
(HO)
(c:/TeXLive/2020/texmf-dist/tex/latex/graphics/lscape.sty
Package: lscape 2000/10/22 v3.01 Landscape Pages (DPC)
)
Package pdflscape Info: Auto-detected driver: pdftex on input line 81.
) (c:/TeXLive/2020/texmf-dist/tex/latex/xcolor/xcolor.sty
Package: xcolor 2016/05/11 v2.12 LaTeX color extensions (UK)
(c:/TeXLive/2020/texmf-dist/tex/latex/graphics-cfg/color.cfg
File: color.cfg 2016/01/02 v1.6 sample color configuration
)
Package xcolor Info: Driver file: pdftex.def on input line 225.
Package xcolor Info: Model `cmy' substituted by `cmy0' on input line
1348.
Package xcolor Info: Model `hsb' substituted by `rgb' on input line 1352.
Package xcolor Info: Model `RGB' extended on input line 1364.
Package xcolor Info: Model `HTML' substituted by `rgb' on input line
1366.
Package xcolor Info: Model `Hsb' substituted by `hsb' on input line 1367.
Package xcolor Info: Model `tHsb' substituted by `hsb' on input line
1368.
Package xcolor Info: Model `HSB' substituted by `hsb' on input line 1369.
Package xcolor Info: Model `Gray' substituted by `gray' on input line
1370.
Package xcolor Info: Model `wave' substituted by `hsb' on input line
1371.
(c:/TeXLive/2020/texmf-dist/tex/latex/graphics/dvipsnam.def
File: dvipsnam.def 2016/06/17 v3.0m Driver-dependent file (DPC,SPQR)
)) (c:/TeXLive/2020/texmf-dist/tex/latex/tools/tabularx.sty
Package: tabularx 2020/01/15 v2.11c `tabularx' package (DPC)
(c:/TeXLive/2020/texmf-dist/tex/latex/tools/array.sty
Package: array 2019/08/31 v2.4l Tabular extension package (FMi)
\col@sep=\dimen165
\ar@mcellbox=\box50
\extrarowheight=\dimen166
\NC@list=\toks22
\extratabsurround=\skip60
\backup@length=\skip61
\ar@cellbox=\box51
)
\TX@col@width=\dimen167
\TX@old@table=\dimen168
\TX@old@col=\dimen169
\TX@target=\dimen170
\TX@delta=\dimen171
\TX@cols=\count270
\TX@ftn=\toks23
) (c:/TeXLive/2020/texmf-dist/tex/latex/threeparttable/threeparttable.sty
Package: threeparttable 2003/06/13  v 3.0
```

```
\@tempboxb=\box52
) (c:/TeXLive/2020/texmf-dist/tex/latex/booktabs/booktabs.sty
Package: booktabs 2020/01/12 v1.61803398 Publication quality tables
\heavyrulewidth=\dimen172
\lightrulewidth=\dimen173
\cmidrulewidth=\dimen174
\belowrulesep=\dimen175
\belowbottomsep=\dimen176
\aboverulesep=\dimen177
\abovetopsep=\dimen178
\cmidrulesep=\dimen179
\cmidrulekern=\dimen180
\defaultaddspace=\dimen181
\@cmidla=\count271
\@cmidlb=\count272
\@aboverulesep=\dimen182
\@belowrulesep=\dimen183
\@thisruleclass=\count273
\@lastruleclass=\count274
\@thisrulewidth=\dimen184
) (c:/TeXLive/2020/texmf-dist/tex/latex/colortbl/colortbl.sty
Package: colortbl 2020/01/04 v1.0e Color table columns (DPC)
\everycr=\toks24
\minrowclearance=\skip62
) (c:/TeXLive/2020/texmf-dist/tex/generic/mathabx/mathabx.sty
Package: mathabx 2003/07/29 v0.0 Non-standard LaTeX package mathabx
\symmatha=\mathgroup4
\symmathb=\mathgroup5
\symmathx=\mathgroup6
(c:/TeXLive/2020/texmf-dist/tex/generic/mathabx/mathabx.dcl
LaTeX Font Info:    Redeclaring math symbol \cdotp on input line 25.
LaTeX Font Info:    Redeclaring math symbol \times on input line 33.
LaTeX Font Info:    Redeclaring math symbol \div on input line 34.
LaTeX Font Info:    Redeclaring math symbol \cdot on input line 35.
LaTeX Font Info:    Redeclaring math symbol \circ on input line 36.
LaTeX Font Info:    Redeclaring math symbol \ast on input line 38.
LaTeX Font Info:    Redeclaring math symbol \pm on input line 41.
LaTeX Font Info:    Redeclaring math symbol \mp on input line 42.
LaTeX Font Info:    Redeclaring math symbol \diamond on input line 45.
LaTeX Font Info:    Redeclaring math symbol \bullet on input line 46.
LaTeX Font Info:    Redeclaring math symbol \star on input line 47.
LaTeX Font Info:    Redeclaring math symbol \amalg on input line 51.
LaTeX Font Info:    Redeclaring math symbol \equiv on input line 83.
LaTeX Font Info:    Redeclaring math symbol \sim on input line 84.
LaTeX Font Info:    Redeclaring math symbol \approx on input line 85.
LaTeX Font Info:    Redeclaring math symbol \simeq on input line 86.
LaTeX Font Info:    Redeclaring math symbol \asymp on input line 89.
LaTeX Font Info:    Redeclaring math symbol \neg on input line 134.
LaTeX Font Info:    Redeclaring math symbol \ll on input line 136.
LaTeX Font Info:    Redeclaring math symbol \gg on input line 137.
LaTeX Font Info:    Redeclaring math symbol \vdash on input line 139.
LaTeX Font Info:    Redeclaring math symbol \dashv on input line 140.
LaTeX Font Info:    Redeclaring math symbol \flat on input line 158.
LaTeX Font Info:    Redeclaring math symbol \natural on input line 159.
```

```
LaTeX Font Info:    Redeclaring math symbol \sharp on input line 160.
LaTeX Font Info:    Redeclaring math symbol \infty on input line 161.
LaTeX Font Info:    Redeclaring math symbol \propto on input line 162.
LaTeX Font Info:    Redeclaring math symbol \dagger on input line 163.
LaTeX Font Info:    Redeclaring math symbol \ddagger on input line 164.
LaTeX Font Info:    Redeclaring math symbol \smile on input line 171.
LaTeX Font Info:    Redeclaring math symbol \frown on input line 172.
LaTeX Font Info:    Redeclaring math accent \dot on input line 193.
LaTeX Font Info:    Redeclaring math accent \ddot on input line 195.
LaTeX Font Info:    Redeclaring math symbol \setminus on input line 218.
LaTeX Font Info:    Redeclaring math symbol \mid on input line 222.
LaTeX Font Info:    Redeclaring math symbol \forall on input line 279.
LaTeX Font Info:    Redeclaring math symbol \partial on input line 281.
LaTeX Font Info:    Redeclaring math symbol \exists on input line 284.
LaTeX Font Info:    Redeclaring math symbol \emptyset on input line 288.
LaTeX Font Info:    Redeclaring math symbol \top on input line 290.
LaTeX Font Info:    Redeclaring math symbol \bot on input line 291.
LaTeX Font Info:    Redeclaring math symbol \perp on input line 292.
LaTeX Font Info:    Redeclaring math symbol \in on input line 299.
LaTeX Font Info:    Redeclaring math symbol \owns on input line 300.
LaTeX Font Info:    Redeclaring math symbol \cap on input line 312.
LaTeX Font Info:    Redeclaring math symbol \cup on input line 313.
LaTeX Font Info:    Redeclaring math symbol \uplus on input line 314.
LaTeX Font Info:    Redeclaring math symbol \sqcap on input line 315.
LaTeX Font Info:    Redeclaring math symbol \sqcup on input line 316.
LaTeX Font Info:    Redeclaring math symbol \wedge on input line 318.
LaTeX Font Info:    Redeclaring math symbol \vee on input line 320.
LaTeX Font Info:    Redeclaring math symbol \subset on input line 344.
LaTeX Font Info:    Redeclaring math symbol \supset on input line 345.
LaTeX Font Info:    Redeclaring math symbol \subseteq on input line 348.
LaTeX Font Info:    Redeclaring math symbol \supseteq on input line 349.
LaTeX Font Info:    Redeclaring math symbol \sqsubseteq on input line
380.
LaTeX Font Info:    Redeclaring math symbol \sqsupseteq on input line
381.
LaTeX Font Info:    Redeclaring math symbol \triangleleft on input line
407.
LaTeX Font Info:    Redeclaring math symbol \triangleright on input line
409.
LaTeX Font Info:    Redeclaring math symbol \leq on input line 439.
LaTeX Font Info:    Redeclaring math symbol \geq on input line 441.
LaTeX Font Info:    Redeclaring math symbol \prec on input line 498.
LaTeX Font Info:    Redeclaring math symbol \succ on input line 499.
LaTeX Font Info:    Redeclaring math symbol \preceq on input line 506.
LaTeX Font Info:    Redeclaring math symbol \succeq on input line 507.
LaTeX Font Info:    Redeclaring math symbol \leftarrow on input line 540.
LaTeX Font Info:    Redeclaring math symbol \rightarrow on input line
542.
LaTeX Font Info:    Redeclaring math symbol \nwarrow on input line 546.
LaTeX Font Info:    Redeclaring math symbol \nearrow on input line 547.
LaTeX Font Info:    Redeclaring math symbol \swarrow on input line 548.
LaTeX Font Info:    Redeclaring math symbol \searrow on input line 549.
LaTeX Font Info:    Redeclaring math symbol \leftrightarrow on input line
550.
```

```
LaTeX Font Info:    Redeclaring math symbol \mapstochar on input line
557.
LaTeX Font Info:    Redeclaring math symbol \leftharpoonup on input line
560.
LaTeX Font Info:    Redeclaring math symbol \rightharpoonup on input line
561.
LaTeX Font Info:    Redeclaring math symbol \leftharpoondown on input
line 562.

LaTeX Font Info:    Redeclaring math symbol \rightharpoondown on input
line 563
.
LaTeX Font Info:    Redeclaring math symbol \Leftarrow on input line 575.
LaTeX Font Info:    Redeclaring math symbol \Rightarrow on input line
576.
LaTeX Font Info:    Redeclaring math symbol \Leftrightarrow on input line
579.
LaTeX Font Info:    Redeclaring math symbol \rhook on input line 612.
LaTeX Font Info:    Redeclaring math symbol \lhook on input line 613.
LaTeX Font Info:    Redeclaring math symbol \oplus on input line 658.
LaTeX Font Info:    Redeclaring math symbol \ominus on input line 659.
LaTeX Font Info:    Redeclaring math symbol \otimes on input line 661.
LaTeX Font Info:    Redeclaring math symbol \odot on input line 663.
LaTeX Font Info:    Redeclaring math symbol \oslash on input line 675.
\mayacnter=\count275
\mayacnta=\count276
\mayacntb=\count277
\mayacntc=\count278
\mayawidth=\dimen185
LaTeX Font Info:    Redeclaring math symbol \intop on input line 753.
LaTeX Font Info:    Redeclaring math symbol \ointop on input line 760.
LaTeX Font Info:    Redeclaring math delimiter \lbrace on input line 842.
LaTeX Info: Redefining \{ on input line 846.
LaTeX Font Info:    Redeclaring math delimiter \rbrace on input line 848.
LaTeX Info: Redefining \} on input line 852.
LaTeX Font Info:    Redeclaring math delimiter \langle on input line 858.
LaTeX Font Info:    Redeclaring math delimiter \rangle on input line 859.
LaTeX Font Info:    Redeclaring math delimiter \vert on input line 863.
LaTeX Font Info:    Redeclaring math delimiter \Vert on input line 865.
LaTeX Font Info:    Redeclaring math delimiter \uparrow on input line
868.
LaTeX Font Info:    Redeclaring math delimiter \downarrow on input line
869.
LaTeX Font Info:    Redeclaring math delimiter \updownarrow on input line
870.
LaTeX Font Info:    Redeclaring math delimiter \Uparrow on input line
871.
LaTeX Font Info:    Redeclaring math delimiter \Downarrow on input line
872.
LaTeX Font Info:    Redeclaring math delimiter \Updownarrow on input line
873.
LaTeX Font Info:    Redeclaring math delimiter \lgroup on input line 880.
LaTeX Font Info:    Redeclaring math delimiter \rgroup on input line 881.
LaTeX Font Info:    Redeclaring math delimiter \lceil on input line 882.
```

```
LaTeX Font Info:    Redeclaring math delimiter \rceil on input line 883.
LaTeX Font Info:    Redeclaring math delimiter \lfloor on input line 884.
LaTeX Font Info:    Redeclaring math delimiter \rfloor on input line 885.
LaTeX Font Info:    Redeclaring math symbol \braceld on input line 903.
LaTeX Font Info:    Redeclaring math symbol \bracerd on input line 905.
LaTeX Font Info:    Redeclaring math symbol \bracelu on input line 907.
LaTeX Font Info:    Redeclaring math symbol \braceru on input line 909.
LaTeX Font Info:    Redeclaring math accent \widehat on input line 944.
LaTeX Font Info:    Redeclaring math accent \widetilde on input line 946.
)) (c:/TeXLive/2020/texmf-dist/tex/latex/hyperref/hyperref.sty
Package: hyperref 2020/01/14 v7.00d Hypertext links for LaTeX
(c:/TeXLive/2020/texmf-dist/tex/generic/ltxcmds/ltxcmds.sty
Package: ltxcmds 2019/12/15 v1.24 LaTeX kernel commands for general use
(HO)
) (c:/TeXLive/2020/texmf-dist/tex/latex/pdftexcmds/pdftexcmds.sty
Package: pdftexcmds 2019/11/24 v0.31 Utility functions of pdfTeX for
LuaTeX (HO
)
(c:/TeXLive/2020/texmf-dist/tex/generic/infwarerr/infwarerr.sty
Package: infwarerr 2019/12/03 v1.5 Providing info/warning/error messages
(HO)
)
Package pdftexcmds Info: \pdf@primitive is available.
Package pdftexcmds Info: \pdf@ifprimitive is available.
Package pdftexcmds Info: \pdfdraftmode found.
) (c:/TeXLive/2020/texmf-dist/tex/generic/kvsetkeys/kvsetkeys.sty
Package: kvsetkeys 2019/12/15 v1.18 Key value parser (HO)
) (c:/TeXLive/2020/texmf-dist/tex/generic/kvdefinekeys/kvdefinekeys.sty
Package: kvdefinekeys 2019-12-19 v1.6 Define keys (HO)
) (c:/TeXLive/2020/texmf-dist/tex/generic/pdfescape/pdfescape.sty
Package: pdfescape 2019/12/09 v1.15 Implements pdfTeX's escape features
(HO)
) (c:/TeXLive/2020/texmf-dist/tex/latex/hycolor/hycolor.sty
Package: hycolor 2020-01-27 v1.10 Color options for hyperref/bookmark
(HO)
) (c:/TeXLive/2020/texmf-dist/tex/latex/letltxmacro/letltxmacro.sty
Package: letltxmacro 2019/12/03 v1.6 Let assignment for LaTeX macros (HO)
) (c:/TeXLive/2020/texmf-dist/tex/latex/auxhook/auxhook.sty
Package: auxhook 2019-12-17 v1.6 Hooks for auxiliary files (HO)
) (c:/TeXLive/2020/texmf-dist/tex/latex/kvoptions/kvoptions.sty
Package: kvoptions 2019/11/29 v3.13 Key value format for package options
(HO)
)
\@linkdim=\dimen186
\Hy@linkcounter=\count279
\Hy@pagecounter=\count280
(c:/TeXLive/2020/texmf-dist/tex/latex/hyperref/pd1enc.def
File: pd1enc.def 2020/01/14 v7.00d Hyperref: PDFDocEncoding definition
(HO)
Now handling font encoding PD1 ...
... no UTF-8 mapping file for font encoding PD1
) (c:/TeXLive/2020/texmf-dist/tex/generic/intcalc/intcalc.sty
Package: intcalc 2019/12/15 v1.3 Expandable calculations with integers
(HO)
```

```
) (c:/TeXLive/2020/texmf-dist/tex/generic/etexcmds/etexcmds.sty
Package: etexcmds 2019/12/15 v1.7 Avoid name clashes with e-TeX commands
(HO)
)
\Hy@SavedSpaceFactor=\count281
Package hyperref Info: Hyper figures OFF on input line 4547.
Package hyperref Info: Link nesting OFF on input line 4552.
Package hyperref Info: Hyper index ON on input line 4555.
Package hyperref Info: Plain pages OFF on input line 4562.
Package hyperref Info: Backreferencing OFF on input line 4567.
Package hyperref Info: Implicit mode ON; LaTeX internals redefined.
Package hyperref Info: Bookmarks ON on input line 4800.
\c@Hy@tempcnt=\count282
(c:/TeXLive/2020/texmf-dist/tex/latex/url/url.sty
\Urlmuskip=\muskip16
Package: url 2013/09/16  ver 3.4  Verb mode for urls, etc.
)
LaTeX Info: Redefining \url on input line 5159.
\XeTeXLinkMargin=\dimen187
(c:/TeXLive/2020/texmf-dist/tex/generic/bitset/bitset.sty
Package: bitset 2019/12/09 v1.3 Handle bit-vector datatype (HO)
(c:/TeXLive/2020/texmf-dist/tex/generic/bigintcalc/bigintcalc.sty
Package: bigintcalc 2019/12/15 v1.5 Expandable calculations on big
integers (HO
)
))
\Fld@menulength=\count283
\Field@Width=\dimen188
\Fld@charsize=\dimen189
Package hyperref Info: Hyper figures OFF on input line 6430.
Package hyperref Info: Link nesting OFF on input line 6435.
Package hyperref Info: Hyper index ON on input line 6438.
Package hyperref Info: backreferencing OFF on input line 6445.
Package hyperref Info: Link coloring OFF on input line 6450.
Package hyperref Info: Link coloring with OCG OFF on input line 6455.
Package hyperref Info: PDF/A mode OFF on input line 6460.
LaTeX Info: Redefining \ref on input line 6500.
LaTeX Info: Redefining \pageref on input line 6504.
(c:/TeXLive/2020/texmf-dist/tex/generic/atbegshi/atbegshi.sty
Package: atbegshi 2019/12/05 v1.19 At begin shipout hook (HO)
)
\Hy@abspage=\count284
\c@Item=\count285
\c@Hfootnote=\count286
)
Package hyperref Info: Driver (autodetected): hpdftex.
(c:/TeXLive/2020/texmf-dist/tex/latex/hyperref/hpdftex.def
File: hpdftex.def 2020/01/14 v7.00d Hyperref driver for pdfTeX
(c:/TeXLive/2020/texmf-dist/tex/latex/atveryend/atveryend.sty
Package: atveryend 2019-12-11 v1.11 Hooks at the very end of document
(HO)
Package atveryend Info: \enddocument detected (standard20110627).
)
\Fld@listcount=\count287
```

```
\c@bookmark@seq@number=\count288
(c:/TeXLive/2020/texmf-dist/tex/latex/rerunfilecheck/rerunfilecheck.sty
Package: rerunfilecheck 2019/12/05 v1.9 Rerun checks for auxiliary files
(HO)
(c:/TeXLive/2020/texmf-dist/tex/generic/uniquecounter/uniquecounter.sty
Package: uniquecounter 2019/12/15 v1.4 Provide unlimited unique counter
(HO)
)
Package uniquecounter Info: New unique counter `rerunfilecheck' on input
line 2
86.
)
\Hy@SectionHShift=\skip63
) (c:/TeXLive/2020/texmf-dist/tex/latex/l3backend/l3backend-pdfmode.def
File: l3backend-pdfmode.def 2020-05-05 L3 backend support: PDF mode
\l__kernel_color_stack_int=\count289
\l__pdf_internal_box=\box53
) (./Manuscript_20201211.aux
LaTeX Font Info:    Trying to load font information for LGI+fib on input
line 7
0.
(c:/TeXLive/2020/texmf-dist/tex/latex/ibycus-babel/lgifib.fd
File: lgifib.fd 2005/11/23 v3.0 (PH/WaS)
))
\openout1 = `Manuscript_20201211.aux'.

LaTeX Font Info:    Checking defaults for OML/cmm/m/it on input line 29.
LaTeX Font Info:    ... okay on input line 29.
LaTeX Font Info:    Checking defaults for OMS/cmsy/m/n on input line 29.
LaTeX Font Info:    ... okay on input line 29.
LaTeX Font Info:    Checking defaults for OT1/cmr/m/n on input line 29.
LaTeX Font Info:    ... okay on input line 29.
LaTeX Font Info:    Checking defaults for T1/cmr/m/n on input line 29.
LaTeX Font Info:    ... okay on input line 29.
LaTeX Font Info:    Checking defaults for TS1/cmr/m/n on input line 29.
LaTeX Font Info:    ... okay on input line 29.
LaTeX Font Info:    Checking defaults for OMX/cmex/m/n on input line 29.
LaTeX Font Info:    ... okay on input line 29.
LaTeX Font Info:    Checking defaults for U/mathx/m/n on input line 29.
LaTeX Font Info:    ... okay on input line 29.
LaTeX Font Info:    Checking defaults for LGI/fib/m/n on input line 29.
LaTeX Font Info:    ... okay on input line 29.
LaTeX Font Info:    Checking defaults for PD1/pdf/m/n on input line 29.
LaTeX Font Info:    ... okay on input line 29.
(c:/TeXLive/2020/texmf-dist/tex/context/base/mkii/supp-pdf.mkii
[Loading MPS to PDF converter (version 2006.09.02).]
\scratchcounter=\count290
\scratchdimen=\dimen190
\scratchbox=\box54
\nofMPsegments=\count291
\nofMParguments=\count292
\everyMPshowfont=\toks25
\MPscratchCnt=\count293
\MPscratchDim=\dimen191
```

```
\MPnumerator=\count294
\makeMPintoPDFobject=\count295
\everyMPtoPDFconversion=\toks26
) (c:/TeXLive/2020/texmf-dist/tex/latex/epstopdf-pkg/epstopdf-base.sty
Package: epstopdf-base 2020-01-24 v2.11 Base part for package epstopdf
Package epstopdf-base Info: Redefining graphics rule for `.eps' on input
line 4
85.
(c:/TeXLive/2020/texmf-dist/tex/latex/latexconfig/epstopdf-sys.cfg
File: epstopdf-sys.cfg 2010/07/13 v1.3 Configuration of (r)epstopdf for
TeX Liv
e
))
*geometry* driver: auto-detecting
*geometry* detected driver: pdftex
*geometry* verbose mode - [ preamble ] result:
* driver: pdftex
* paper: custom
* layout: <same size as paper>
* layoutoffset:(h,v)=(0.0pt,0.0pt)
* hratio: 1:1
* vratio: 1:1
* modes:
* h-part:(L,W,R)=(64.75394pt, 468.0pt, 64.75394pt)
* v-part:(T,H,B)=(111.52342pt, 622.0pt, 111.52342pt)
* \paperwidth=597.50787pt
* \paperheight=845.04684pt
* \textwidth=468.0pt
* \textheight=622.0pt
* \oddsidemargin=-7.51605pt
* \evensidemargin=-7.51605pt
* \topmargin=-22.74657pt
* \headheight=50.0pt
* \headsep=12.0pt
* \topskip=10.0pt
* \footskip=12.0pt
* \marginparwidth=4.0pt
* \marginparsep=10.0pt
* \columnsep=24.0pt
* \skip\footins=24.0pt plus 2.0pt minus 12.0pt
* \hoffset=0.0pt
* \voffset=0.0pt
* \mag=1000
* \@twocolumntrue
* \@twosidefalse
* \@mparswitchfalse
* \@reversemarginfalse
* (1in=72.27pt=25.4mm, 1cm=28.453pt)

Package caption Info: Begin \AtBeginDocument code.
Package caption Info: subfig package v1.3 is loaded.
Package caption Info: hyperref package is loaded.
Package caption Info: threeparttable package is loaded.
Package caption Info: End \AtBeginDocument code.
```

```
\AtBeginShipoutBox=\box55
Package hyperref Info: Link coloring OFF on input line 29.
(c:/TeXLive/2020/texmf-dist/tex/latex/hyperref/nameref.sty
Package: nameref 2019/09/16 v2.46 Cross-referencing by name of section
(c:/TeXLive/2020/texmf-dist/tex/latex/refcount/refcount.sty
Package: refcount 2019/12/15 v3.6 Data extraction from label references
(HO)
) (c:/TeXLive/2020/texmf-
dist/tex/generic/gettitlestring/gettitlestring.sty
Package: gettitlestring 2019/12/15 v1.6 Cleanup title references (HO)
)
\c@section@level=\count296
)
LaTeX Info: Redefining \ref on input line 29.
LaTeX Info: Redefining \pageref on input line 29.
LaTeX Info: Redefining \nameref on input line 29.
(./Manuscript_20201211.out) (./Manuscript_20201211.out)
\@outlinefile=\write4
\openout4 = `Manuscript_20201211.out'.

LaTeX Font Info:    External font `cmex10' loaded for size
(Font)              <7> on input line 60.
LaTeX Font Info:    External font `cmex10' loaded for size
(Font)              <5> on input line 60.
! Undefined control sequence.
l.67 \newpageafter
                  {abstract}
The control sequence at the end of the top line
of your error message was never \def'ed. If you have
misspelled it (e.g., `\hobx'), type `I' and the correct
spelling (e.g., `I\hbox'). Otherwise just continue,
and I'll forget about whatever was undefined.

[1

{c:/TeXLive/2020/texmf-var/fonts/map/pdftex/updmap/pdftex.map}

]
LaTeX Font Info:    External font `cmex10' loaded for size
(Font)              <8> on input line 69.
LaTeX Font Info:    External font `cmex10' loaded for size
(Font)              <6> on input line 69.

Package natbib Warning: Citation `ainsbury2016ionizing' on page 2
undefined on
input line 72.


Package natbib Warning: Citation `uwineza2019cataractogenic' on page 2
undefine
d on input line 72.
```

```
Package natbib Warning: Citation `gajewski1977types' on page 2 undefined
on inp
ut line 75.


Package natbib Warning: Citation `de2015patched' on page 2 undefined on
input l
ine 77.


Package natbib Warning: Citation `gorgels2007retinal' on page 2 undefined
on in
put line 106.


Package natbib Warning: Citation `lucas1961effect' on page 2 undefined on
input
 line 107.


Package natbib Warning: Citation `schmidt2001effects' on page 2 undefined
on in
put line 107.


Package natbib Warning: Citation `borges2004radiation' on page 2
undefined on i
nput line 107.


Package natbib Warning: Citation `gajewski1977types' on page 2 undefined
on inp
ut line 110.


Underfull \hbox (badness 10000) in paragraph at lines 72--114

 []


Underfull \hbox (badness 1616) in paragraph at lines 72--114
\OT1/cmr/m/n/10 P4-irradiated mice (CBA/H strain), ir-ra-di-ated
 []


Underfull \hbox (badness 10000) in paragraph at lines 72--114

 []


Underfull \hbox (badness 4713) in paragraph at lines 72--114
\OT1/cmr/m/n/10 In the cur-rent study, we demon-strate that
 []
```

```
Underfull \hbox (badness 2865) in paragraph at lines 72--114
\OT1/cmr/m/n/10 op-ti-cal co-her-ence to-mog-ra-phy (OCT) for the
 []


Underfull \hbox (badness 2326) in paragraph at lines 72--114
\OT1/cmr/m/n/10 imag-ing for the den-sity quan-tifi-ca-tion of the
 []


Underfull \hbox (badness 2351) in paragraph at lines 72--114
\OT1/cmr/m/n/10 re-gard-ing the phe-no-type of radiation-impaired
 []


Underfull \hbox (badness 1622) in paragraph at lines 72--114
\OT1/cmr/m/n/10 murine neona-tal reti-nae by quan-tifi-ca-tion and
 []


Underfull \vbox (badness 10000) has occurred while \output is active []

[2

]

LaTeX Warning: `!h' float specifier changed to `!ht'.


Package natbib Warning: Citation `kunze2015new' on page 3 undefined on
input li
ne 116.


Package natbib Warning: Citation `dalke2018lifetime' on page 3 undefined
on inp
ut line 116.


Package natbib Warning: Citation `puk2009reduced' on page 3 undefined on
input
line 122.


Underfull \hbox (badness 4739) in paragraph at lines 122--123
[]\OT1/cmr/m/n/10 The lens opac-ity was anal-ysed us-ing the
 []


Package natbib Warning: Citation `pawliczek2019spectral' on page 3
undefined on
 input line 124.
```

```
Package natbib Warning: Citation `puk2013longitudinal' on page 3
undefined on i
nput line 124.


Underfull \hbox (badness 1092) in paragraph at lines 124--128
\OT1/cmr/m/n/10 OCT and Scheimpflug data were de-posited in
 []

[3]

Package natbib Warning: Citation `prusky2004rapid' on page 4 undefined on
input
 line 129.


Underfull \hbox (badness 1087) in paragraph at lines 131--135
\OT1/cmr/m/n/10 calretinin (Swant, 7699/3H, 1:100), anti-GFAP
 []


Underfull \hbox (badness 10000) in paragraph at lines 131--135

 []

<Figure_1.png, id=99, 430.7292pt x 149.358pt>
File: Figure_1.png Graphic file (type png)
<use Figure_1.png>
Package pdftex.def Info: Figure_1.png  used on input line 140.
(pdftex.def)             Requested size: 455.24408pt x 157.86063pt.

LaTeX Warning: `h' float specifier changed to `ht'.


LaTeX Warning: `!h' float specifier changed to `!ht'.

<Figure_2.png, id=101, 424.9476pt x 132.0132pt>
File: Figure_2.png Graphic file (type png)
<use Figure_2.png>
Package pdftex.def Info: Figure_2.png  used on input line 181.
(pdftex.def)             Requested size: 398.33858pt x 123.74796pt.

LaTeX Warning: `!h' float specifier changed to `!ht'.

<Figure_3.png, id=106, 380.622pt x 146.4672pt>
File: Figure_3.png Graphic file (type png)
<use Figure_3.png>
Package pdftex.def Info: Figure_3.png  used on input line 189.
(pdftex.def)             Requested size: 213.39566pt x 82.11716pt.

LaTeX Warning: `!h' float specifier changed to `!ht'.
```

```
Overfull \hbox (0.58102pt too wide) in paragraph at lines 197--218
[]
 []


LaTeX Warning: `h' float specifier changed to `ht'.

<Figure_4.png, id=112, 475.0548pt x 279.444pt>
File: Figure_4.png Graphic file (type png)
<use Figure_4.png>
Package pdftex.def Info: Figure_4.png  used on input line 224.
(pdftex.def)             Requested size: 455.24408pt x 267.80267pt.
<Figure_5.png, id=113, 461.5644pt x 357.4956pt>
File: Figure_5.png Graphic file (type png)
<use Figure_5.png>
Package pdftex.def Info: Figure_5.png  used on input line 232.
(pdftex.def)             Requested size: 455.24408pt x 352.59618pt.
<Figure_6.png, id=122, 457.71pt x 291.9708pt>
File: Figure_6.png Graphic file (type png)
<use Figure_6.png>
Package pdftex.def Info: Figure_6.png  used on input line 250.
(pdftex.def)             Requested size: 455.24408pt x 290.41078pt.

Underfull \hbox (badness 1867) in paragraph at lines 219--257
\OT1/cmr/m/n/10 lenses with OCT, con-ducted 2.5 months p.i.,
 []


Underfull \hbox (badness 10000) in paragraph at lines 219--257

 []


Underfull \hbox (badness 5519) in paragraph at lines 219--257
\OT1/cmr/m/n/10 radiation dis-played a sim-i-lar dis-tri-bu-tion of
 []


Underfull \hbox (badness 10000) in paragraph at lines 219--257

 []


Underfull \hbox (badness 1005) in paragraph at lines 219--257
\OT1/cmr/m/n/10 In ad-di-tion to the enu-mer-ated cataract types,
 []


Underfull \hbox (badness 1178) in paragraph at lines 219--257
\OT1/cmr/m/n/10 im-ages of the ex-tru-sion, a bolt-like scat-ter-ing
 []


Underfull \hbox (badness 1681) in paragraph at lines 219--257
```

```
\OT1/cmr/m/n/10 ex-tru-sions oc-curred in fe-male WTs and male
 []


LaTeX Warning: `h' float specifier changed to `ht'.


LaTeX Warning: `!h' float specifier changed to `!ht'.

[4]
Underfull \vbox (badness 10000) has occurred while \output is active []


Underfull \vbox (badness 10000) has occurred while \output is active []

[5 <./Figure_1.png>]

LaTeX Warning: `h' float specifier changed to `ht'.


Underfull \hbox (badness 2027) in paragraph at lines 258--262
 []\OT1/cmr/m/it/10 Scheimpflug imag-ing.[] \OT1/cmr/m/n/10 In a sec-ond
\OT1/c
mr/m/it/10 in-vivo \OT1/cmr/m/n/10 ap-
 []


Underfull \hbox (badness 4429) in paragraph at lines 258--262
\OT1/cmr/m/n/10 proach, we mon-i-tored all an-i-mals with the
 []


Underfull \hbox (badness 1107) in paragraph at lines 263--283
\OT1/cmr/m/n/10 Besides that, the in-ner nu-clear layer and the
 []


Underfull \hbox (badness 1342) in paragraph at lines 263--283
\OT1/cmr/m/n/10 were com-pletely de-prived of pho-tore-cep-tors as
 []


Underfull \hbox (badness 2142) in paragraph at lines 263--283
\OT1/cmr/m/n/10 photoreceptor-depleted zones around the op-tic
 []


Underfull \hbox (badness 10000) in paragraph at lines 263--283

 []


Underfull \hbox (badness 10000) in paragraph at lines 263--283
```

```
 []


Underfull \hbox (badness 2401) in paragraph at lines 263--283
\OT1/cmr/m/n/10 by inflammation-related in-crease in ex-pres-sion
 []

[6 <./Figure_2.png> <./Figure_3.png>]
Underfull \vbox (badness 10000) has occurred while \output is active []


Underfull \vbox (badness 10000) has occurred while \output is active []

[7 <./Figure_4.png>]
Underfull \vbox (badness 10000) has occurred while \output is active []


Underfull \vbox (badness 10000) has occurred while \output is active []

[8 <./Figure_5.png>]
<Figure_7.png, id=196, 456.7464pt x 198.0198pt>
File: Figure_7.png Graphic file (type png)
<use Figure_7.png>
Package pdftex.def Info: Figure_7.png  used on input line 287.
(pdftex.def)             Requested size: 455.24408pt x 171.85435pt.
<Figure_8.png, id=198, 456.2646pt x 145.9854pt>
File: Figure_8.png Graphic file (type png)
<use Figure_8.png>
Package pdftex.def Info: Figure_8.png  used on input line 295.
(pdftex.def)             Requested size: 455.24408pt x 145.66203pt.

Underfull \hbox (badness 10000) in paragraph at lines 284--304

 []


Underfull \hbox (badness 1043) in paragraph at lines 284--304
\OT1/cmr/m/n/10 might cor-re-late with the im-pair-ment of vi-sual
 []


LaTeX Warning: `h' float specifier changed to `ht'.


LaTeX Warning: `!h' float specifier changed to `!ht'.


Underfull \vbox (badness 10000) has occurred while \output is active []

[9 <./Figure_6.png>]
<Figure_9.png, id=207, 344.487pt x 183.084pt>
File: Figure_9.png Graphic file (type png)
<use Figure_9.png>
Package pdftex.def Info: Figure_9.png  used on input line 310.
```

```
(pdftex.def)             Requested size: 213.57973pt x 113.5109pt.
<Figure_10.png, id=208, 867.24pt x 345.9324pt>
File: Figure_10.png Graphic file (type png)
<use Figure_10.png>
Package pdftex.def Info: Figure_10.png  used on input line 318.
(pdftex.def)             Requested size: 459.63503pt x 183.34329pt.

Package natbib Warning: Citation `gajewski1977types' on page 10 undefined
on in
put line 329.


Package natbib Warning: Citation `pei2008correlation' on page 10
undefined on i
nput line 331.


Package natbib Warning: Citation `gajewski1977types' on page 10 undefined
on in
put line 335.


Package natbib Warning: Citation `de2015patched' on page 10 undefined on
input
line 335.


Package natbib Warning: Citation `eisenfeld1984muller' on page 10
undefined on
input line 345.


Package natbib Warning: Citation `dyer2000control' on page 10 undefined
on inpu
t line 345.


Underfull \hbox (badness 1924) in paragraph at lines 305--353
\OT1/cmr/m/n/10 was nat-u-rally prone to mis-judge-ment. Still,
 []


Underfull \hbox (badness 1377) in paragraph at lines 305--353
\OT1/cmr/m/n/10 had a le-sion severity-increasing ef-fect only on
 []


Underfull \hbox (badness 1735) in paragraph at lines 305--353
\OT1/cmr/m/n/10 fea-ture of mice ir-ra-di-ated sev-eral weeks af-ter
 []


Underfull \hbox (badness 10000) in paragraph at lines 305--353
```

```
 []


Underfull \hbox (badness 5696) in paragraph at lines 305--353
\OT1/cmr/m/n/10 Retinal al-ter-ations fol-low-ing ex-po-sure to
$\OML/cmm/m/it/
10 ^^M$\OT1/cmr/m/n/10 -
 []


Underfull \hbox (badness 5175) in paragraph at lines 305--353
\OT1/cmr/m/n/10 thick-ness, mea-sured undis-torted and re-li-ably
 []


Underfull \hbox (badness 2384) in paragraph at lines 305--353
\OT1/cmr/m/n/10 dis-tri-bu-tion over-lap what-so-ever oc-curred (also
 []


Underfull \hbox (badness 1107) in paragraph at lines 305--353
\OT1/cmr/m/n/10 but that ir-ra-di-ated reti-nae shrank faster than
 []


Underfull \hbox (badness 1199) in paragraph at lines 305--353
\OT1/cmr/m/n/10 the ex-pres-sion pat-tern of Sprague-Dawley rats
 []


Underfull \hbox (badness 1184) in paragraph at lines 305--353
\OT1/cmr/m/n/10 from non-regenerating reti-nal tis-sue [\OT1/cmr/bx/n/10
?\OT1/
cmr/m/n/10 ]. The
 []


Underfull \hbox (badness 1184) in paragraph at lines 305--353
\OT1/cmr/m/n/10 en-hanced radiation-related ex-pres-sion of GPX1
 []


Underfull \hbox (badness 10000) in paragraph at lines 305--353

 []


LaTeX Warning: `!h' float specifier changed to `!ht'.


LaTeX Warning: `!h' float specifier changed to `!ht'.


Underfull \vbox (badness 10000) has occurred while \output is active []
```

```
[10 <./Figure_7.png> <./Figure_8.png>] [11 <./Figure_9.png>]
Underfull \vbox (badness 10000) has occurred while \output is active []


Package natbib Warning: Citation `gajewski1977types' on page 12 undefined
on in
put line 354.


Package natbib Warning: Citation `gorgels2007retinal' on page 12
undefined on i
nput line 354.


Package natbib Warning: Citation `hamada2016cataractogenesis' on page 12
undefi
ned on input line 357.


Underfull \hbox (badness 1215) in paragraph at lines 354--358
\OT1/cmr/m/n/10 cor-ti-cal opaci-fi-ca-tion (type II cataracts in 10-
 []


Underfull \hbox (badness 10000) in paragraph at lines 354--358

 []


Underfull \hbox (badness 1867) in paragraph at lines 354--358
\OT1/cmr/m/n/10 Although the trans-fer of murine ex-per-i-men-tal
 []

[12 <./Figure_10.png>]
No file Manuscript_20201211.bbl.

Package natbib Warning: There were undefined citations.

Package atveryend Info: Empty hook `BeforeClearDocument' on input line
371.
[13

]
Package atveryend Info: Empty hook `AfterLastShipout' on input line 371.
(./Manuscript_20201211.aux)
Package atveryend Info: Executing hook `AtVeryEndDocument' on input line
371.
Package atveryend Info: Executing hook `AtEndAfterFileList' on input line
371.
Package rerunfilecheck Info: File `Manuscript_20201211.out' has not
changed.
(rerunfilecheck)             Checksum:
13ADF392F8A42D036920D61F43F0FA77;812.
```

```
LaTeX Warning: Label(s) may have changed. Rerun to get cross-references
right.

Package atveryend Info: Empty hook `AtVeryVeryEnd' on input line 371.
 )
Here is how much of TeX's memory you used:
 10513 strings out of 480681
 154106 string characters out of 5908536
 483444 words of memory out of 5000000
 26056 multiletter control sequences out of 15000+600000
 544450 words of font info for 60 fonts, out of 8000000 for 9000
 1141 hyphenation exceptions out of 8191
 50i,19n,48p,1267b,586s stack positions out of
5000i,500n,10000p,200000b,80000s
{c:/TeXLive/2020/texmf-dist/fonts/enc/dvips/cm-super/cm-super-
ts1.enc}<c:/TeX
Live/2020/texmf-
dist/fonts/type1/public/amsfonts/cm/cmbx10.pfb><c:/TeXLive/2020
/texmf-
dist/fonts/type1/public/amsfonts/cm/cmbx8.pfb><c:/TeXLive/2020/texmf-dis
t/fonts/type1/public/amsfonts/cm/cmmi10.pfb><c:/TeXLive/2020/texmf-
dist/fonts/t
ype1/public/amsfonts/cm/cmmi8.pfb><c:/TeXLive/2020/texmf-
dist/fonts/type1/publi
c/amsfonts/cm/cmr10.pfb><c:/TeXLive/2020/texmf-
dist/fonts/type1/public/amsfonts
/cm/cmr12.pfb><c:/TeXLive/2020/texmf-
dist/fonts/type1/public/amsfonts/cm/cmr7.p
fb><c:/TeXLive/2020/texmf-
dist/fonts/type1/public/amsfonts/cm/cmr8.pfb><c:/TeXL
ive/2020/texmf-
dist/fonts/type1/public/amsfonts/cm/cmss8.pfb><c:/TeXLive/2020/t
exmf-
dist/fonts/type1/public/amsfonts/cm/cmti10.pfb><c:/TeXLive/2020/texmf-
dist
/fonts/type1/public/amsfonts/cm/cmti7.pfb><c:/TeXLive/2020/texmf-
dist/fonts/typ
e1/public/amsfonts/cm/cmti8.pfb><c:/TeXLive/2020/texmf-
dist/fonts/type1/public/
amsfonts/cm/cmtt10.pfb><c:/TeXLive/2020/texmf-
dist/fonts/type1/public/amsfonts/
cm/cmtt8.pfb><c:/TeXLive/2020/texmf-
dist/fonts/type1/public/ibygrk/fibr84.pfb><
c:/TeXLive/2020/texmf-dist/fonts/type1/public/mathabx-
type1/matha10.pfb><c:/TeX
Live/2020/texmf-dist/fonts/type1/public/mathabx-
type1/matha6.pfb><c:/TeXLive/20
20/texmf-dist/fonts/type1/public/mathabx-
type1/matha7.pfb><c:/TeXLive/2020/texm
f-dist/fonts/type1/public/mathabx-
type1/matha8.pfb><c:/TeXLive/2020/texmf-dist/
fonts/type1/public/mathabx-type1/mathb10.pfb><c:/TeXLive/2020/texmf-
dist/fonts/
```

```
type1/public/mathabx-type1/mathb8.pfb><c:/TeXLive/2020/texmf-
dist/fonts/type1/p
ublic/mathabx-type1/mathx10.pfb><c:/TeXLive/2020/texmf-
dist/fonts/type1/public/
cm-super/sfrm0700.pfb><c:/TeXLive/2020/texmf-dist/fonts/type1/public/cm-
super/s
frm1000.pfb>
Output written on Manuscript_20201211.pdf (13 pages, 3453359 bytes).
PDF statistics:
 329 PDF objects out of 1000 (max. 8388607)
 264 compressed objects within 3 object streams
 53 named destinations out of 1000 (max. 500000)
 161 words of extra memory for PDF output out of 10000 (max. 10000000)
```